bachelor's thesis

Predictive Control and Stabilization of a Formation of Quadrotors Filming in Dark Conditions

Vít Krátký

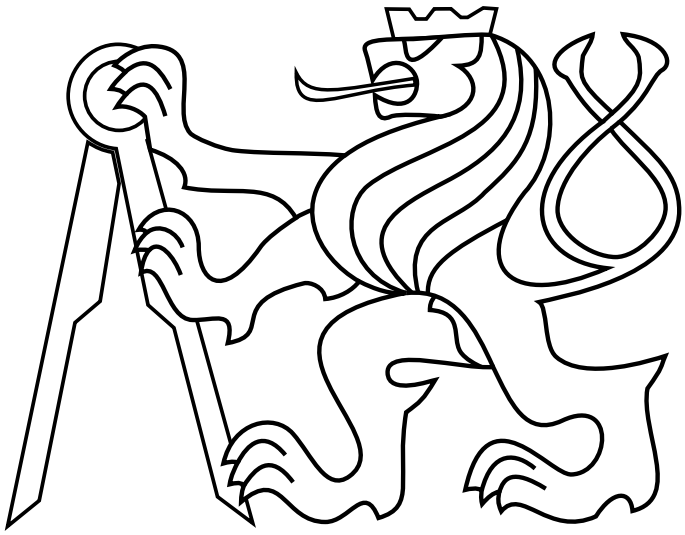

May 2017

Thesis supervisor: Ing. Martin Saska, Dr. rer. nat.

Czech Technical University in Prague
Faculty of Electrical Engineering, Department of Cybernetics

Czech Technical University in Prague
Faculty of Electrical Engineering

Department of Cybernetics

BACHELOR PROJECT ASSIGNMENT

Student: Vít K r á t k ý

Study programme: Cybernetics and Robotics

Specialisation: Robotics

Title of Bachelor Project: Predictive Control and Stabilization of a Formation of Quadrotors Filming in Dark Conditions

Guidelines:

The aim of the thesis is to understand a method designed for stabilization of formations of Unmanned Aerial Vehicles (UAV) [2,3] and adapt it for the task of filming in dark areas, where one UAV carries a camera and neighboring UAVs carry a source of light. Work plan:

- To define the filming technique Three point lighting [1,4] as an optimization problem in the Model Predictive Control (MPC) taking into account constraints of the formation flying.
- To implement an obstacle avoidance method into the MPC control and to extend the algorithm for filming 3D objects (3D formation flying).
- To verify the algorithm in the Gazebo simulator under ROS using maps inspired by deployment of the system in historical buildings. To prepare the system for a real experiment, which will be conducted based on availability of real quadrotors (thesis advisor will decide if the real experiment or a complex statistical analysis in the simulator will be realized).

Bibliography/Sources:

[1] Zhang, Y. - Ma K.L. Lighting design for globally illuminated volume rendering. IEEE Trans Vis Comput Graph. 19(12):2946-55, 2013.
[2] M Saska, V Spurny and V Vonasek. Predictive control and stabilization of nonholonomic formations with integrated spline-path planning. Robotics and Autonomous Systems 75(Part B):379-397, 2016.
[3] M Saska, Z Kasl and L Preucil. Motion Planning and Control of Formations of Micro Aerial Vehicles. In Proceedings of The 19th World Congress of the International Federation of Automatic Control (IFAC). 2014.
[4] Hymann, I. Three point lighting: Learn how to use the key, fill, and back lights. Online tutorial. http://www.izzyvideo.com/three-point-lighting/ [cit. 2016-2-19], 2016.

Bachelor Project Supervisor: Ing. Martin Saska, Dr. rer. nat.

Valid until: the end of the summer semester of academic year 2017/2018

L.S.

prof. Dr. Ing. Jan Kybic
Head of Department

prof. Ing. Pavel Ripka, CSc.
Dean

Prague, February 14, 2017

Declaration

I declare that the presented work was developed independently and that I have listed all sources of information used within it in accordance with the methodical instructions for observing the ethical principles in the preparation of university theses.

Prague, date ....
signature

Acknowledgement

Firstly I would like to thank Dr. Martin Saska and Ing. Vojtěch Spurný for their great support throughout this project. Furthermore, I would also like to thank other people from Multi-robot Systems group for valuable advice and assistance with the realization of the experiments.

Abstrakt

Cílem této práce je navrhnout systém pro autonomní stabilizaci formace vícerotorových helikoptér v úloze kooperativního filmování v šeru. Formace se skládá z vícerotorové helikoptéry nesoucí kameru a libovolného počtu dalších robotů vybavených zdrojem světla. Prezentovaný systém využívá principu lídr-následovník a prediktivního řízení na ustupujícím horizontu. Schéma lídr-následovník je navrženo tak, aby bylo využitelné pro dvě techniky osvětlování - tří bodové osvětlení a razantní boční osvětlení. Součástí systému je vyhýbání se kolizím i další omezení, která činí trajektorie proveditelnými a zvyšují kvalitu získaných záběrů. Navržený systém a jeho možné modifikace, které jsou rovněž prezentovány v této práci, jsou ověřeny v četných simulačních experimentech a také v rámci reálného experimentu v modelovaném venkovním prostředí.

Klíčová slova

multi-robotické formace; stabilizace formace; prediktivní řízení; tří bodové osvětlení

Abstract

The aim of this work is to design the system for autonomous stabilization of a formation of multi-rotor helicopters for the cooperative filming in dark conditions. The leader-follower approach and the model predictive control on receding horizon are applied for this purpose. The formation consists of one multi-rotor helicopter carrying a camera and the arbitrary number of multi-rotors carrying light sources. The leader-follower scheme is proposed in the way, that it is suitable for two lighting techniques - Three point lighting and Strong side lighting. The proposed system also deals with the collision avoidance and take into account other constraints to provide feasible trajectories and good quality of acquired videos or photos. The system and its modifications, which are also presented in this work, are verified in numerous simulation experiments and one real experiment conducted in modeled outdoor environment.

Keywords

multi-robot formation; formation stabilization; model predictive control; three point lighting

Contents

1 Introduction **1**

2 State of the art **2**

3 Problem definition **3**

4 Preliminaries **4**
4.1 Model predictive control 4
4.2 Configuration and parameters of robots 5
4.3 Kinematic model 6
4.4 Three point lighting 7

5 Formation stabilization **8**
5.1 Leader-follower scheme 8
5.2 Scene capturing by leader with camera 9
5.2.1 Trajectory tracking 10
5.2.2 Camera heading control 12
5.3 Scene lighting by followers holding the light 13
5.3.1 Trajectory tracking for followers holding the light 15
5.3.2 Light heading control 17
5.4 Possible modifications and their advantages and disadvantages 18

6 Implementation details **20**
6.1 Sequential quadratic programming 20
6.2 Obstacle avoidance 20

7 Experimental results **21**
7.1 Simulation 21
7.1.1 Experiment in complex environment 21
7.1.2 Experiment with three lights 29
7.1.3 2D-modification - two rooms environment 29
7.1.4 2D-modification - simple environment 34
7.2 Real experiment 36

8 Conclusion **39**

References **40**

Appendices

A CD content **43**

B Additional experimental results **44**

List of Tables

1 The constants used in the optimization task of the leader in the experiment presented in Subsection 7.1.1. 22
2 The constants used in optimization task of the followers in the experiment presented in Subsection 7.1.1. 22
3 The limitations on control inputs used in the experiment presented in Subsection 7.1.1. 22

4 CD content 43

5 The constants used in the optimization task of the leader in the experiment presented in Subsection 7.1.2. 44
6 The constants used in the optimization task of the followers in the experiment presented in Subsection 7.1.2. 44
7 The limitations on control inputs used in the experiment presented in Subsection 7.1.2. 44
8 The constants used in the optimization task of the leader in the experiment presented in Subsection 7.1.3. 47
9 The constants used in the optimization task of the followers in the experiment presented in Subsection 7.1.3. 47
10 The limitations on the control inputs used for control of the robots in the experiments presented in Subsection 7.1.3 and 7.1.4 48
11 The constants used in the optimization task of the leader in the experiment presented in Subsection 7.1.4. 51
12 The constants used in the optimization task of the followers in the experiment presented in Subsection 7.1.4. 51

List of Figures

1 Deployment of the manually controlled quadrotors for filming. [1] 1

2 The MPC concept, which is used for trajectory following in this work. . 4

3 Illustration of the horizontal angle of view AoV_h, the vertical angle of view AoV_v and the field of view FOV - the parameters of the camera. . 5

4 The common placement of lights in three point lighting technique. . . . 7

5 Illustration of the leader-follower scheme presented in this work. 9

6 The diagram of the part of the proposed system for formation stabilization which is connected with leader. 10

7 The diagram of the part of the proposed system for formation stabilization, which is connected with followers. The process which precedes to the formation driving module is closer described in Fig. 6. 14

8 The influence of the length of control horizon N on the computational time of one step of the optimization process. Values for the "2D" method and the originally presented one (marked as "3D") are presented for comparison of their computational demands. Each value was obtained as the mean from 1000 runs of the algorithm. 18

9 Two types of obstacles considered within the optimization task 20

10 Snapshots of the formation during the change of light angles because of the transition between lighting of the 3D and 2D image. The changes of the vertical lighting angles $\varrho_j(t)$ are accompanied by the change of the altitude of both followers. 23

11 The progress of the values of the objective functions used for trajectory tracking and heading control of particular robots in the experiment presented in Subsection 7.1.1. 24

12 Snapshots of the formation during the transition to another object of interest. The followers use the change of the altitude for avoiding other robots in the formation and the presence in the FOV (in the case of followers). It is more evident from Fig. 15, 16 or the video: `https://youtu.be/OcDyQFgTjcs`. 25

13 Control inputs used for controlling of the robots in the experiment presented in Subsection 7.1.1. 26

14 The trajectory of the leader in the experiment in the complex environment. The arrows denote the heading of the camera at particular times t, and the green dotted line shows the desired trajectory. 27

15 The trajectory of the follower carrying the key light in the experiment in the complex environment. The arrows denote the heading of the light at particular times t. 27

16 The trajectory of the follower carrying the fill light in the experiment in the complex environment. The arrows denote the heading of the light at particular times t. 28
17 Snapshot of the formation with three lights during the scanning of the OoI. The dotted circles highlight the leader (green), the follower provided the key light (blue), the follower provided the fill light (red), and the follower provided the backlight (orange). 29
18 The trajectory of the leader in the experiment with three lights. The arrows denote the heading of the camera at particular times t, and the green dotted line shows the desired trajectory. The trajectories of the followers in this experiment are presented in Fig. 19, 29, 28 in the appendix B. 30
19 The trajectory of the follower carrying the back light in the experiment with three lights (Subsection 7.1.2). The arrows denote the heading of light at particular times t. 30
20 The trajectory of the leader in the "2D experiment". The arrows denote the heading of the camera at particular times t, and the green dotted line shows the desired trajectory. 31
21 Snapshots of the formation during the transition to another OoI and concurrent avoiding to the obstacle in the experiment presented in Subsection 7.1.3. The dotted circles highlight the leader (green), the follower provided the key light (blue), and the follower provided the fill light (red). The corresponding camera shot is shown in the cut-out separated with the red line. (video: `https://youtu.be/jpJzaMv0G8s`) 32
22 Snapshots of the formation during the avoiding the faulty follower. The dotted circles highlight the leader (green), the follower provided the key light (blue), and the follower provided the fill light (red). (video: `https://youtu.be/jpJzaMv0G8s`) 33
23 The trajectory of the leader in the experiment in the simple environment with the obstacle. The arrows denote the heading of the camera at particular times t, and the green dotted line shows the desired trajectory. 35
24 The trajectory of the follower carrying the key light in the experiment in simple environment with the obstacle. The arrows denote the heading of the light at particular times t. 35
25 The multi-rotor helicopter equipped with the light, which was deployed in the real experiment. 36
26 The photos of the formation at particular times of the real experiment (left side) and the photos cut out from the video taken by the camera mounted on the frame of the leader at corresponding times (right side). The dotted circles highlight the leader (green), the follower provided the key light (blue), and the follower provided the fill light (red). (video: `https://youtu.be/CuXX3hlA7Hk`) 37
27 The photos of the formation at particular times of the real experiment (left side) and the photos cut out from the video taken by the camera mounted on the frame of the leader at corresponding times (right side). The dotted circles highlight the leader (green), the follower provided the key light (blue), and the follower provided the fill light (red). (video: `https://youtu.be/CuXX3hlA7Hk`) 38

28 The trajectory of the follower carrying the key light in the experiment with three lights (Subsection 7.1.2). The arrows denote the heading of light at particular times t. 45
29 The trajectory of the follower carrying the fill light in the experiment with three lights (Subsection 7.1.2). The arrows denote the heading of light at particular times t. 45
30 Control inputs used for controlling of the robots in the experiment with three lights presented in Subsection 7.1.2. 46
31 The progress of the values of the objective functions used for trajectory tracking and heading control of particular robots in the experiment with three lights presented in Subsection 7.1.2. 47
32 The trajectory of the follower carrying the key light in the 2D experiment (Subsection 7.1.3). The arrows denote the heading of the light at particular times t. 48
33 The trajectory of the follower carrying the fill light in the 2D experiment (Subsection 7.1.3). The arrows denote the heading of the light at particular times t. 48
34 Control inputs used for controlling of the robots in the experiment presented in Subsection 7.1.3. 49
35 The progress of the values of the objective functions used for trajectory tracking and heading control of particular robots in the experiment presented in Subsection 7.1.3. 50
36 The trajectory of the leader in the experiment with variable segmented trajectory presented in Subsection 7.1.4. The arrows denote the camera heading at particular times t, and the green dotted line shows the desired trajectory. 51
37 The trajectory of the follower carrying the key light in the experiment with variable segmented trajectory presented in Subsection 7.1.4. The arrows denote the heading of the light at particular times t, and the green dotted line shows the desired trajectory. 52
38 The trajectory of the follower carrying the fill light in the experiment with variable segmented trajectory presented in Subsection 7.1.4. The arrows denote the heading of the light at particular times t, and the green dotted line shows the desired trajectory. 52
39 Control inputs used for controlling of robots in the experiment presented in Subsection 7.1.4 - variable segmented trajectory. 53
40 The progress of the values of the objective functions used for trajectory tracking and heading control of particular robots in the experiment presented in Subsection 7.1.4 - variable segmented trajectory. 54
41 The trajectory of the leader in the experiment in simple environment - trajectory with constant step presented in Subsection 7.1.4. The arrows denote the camera heading at particular times t, and the green dotted line shows the desired trajectory. 55
42 The trajectory of the follower carrying the key light in the experiment in simple environment - trajectory with constant step presented in Subsection 7.1.4. The arrows denote the heading of light at particular times t, and the green dotted line shows the desired trajectory. 55

43 The trajectory of the follower carrying the fill light in the experiment in simple environment - trajectory with constant step presented in Subsection 7.1.4. The arrows denote the heading of light at particular times t, and the green dotted line shows the desired trajectory. 56
44 Control inputs used for controlling of the robots in the experiment presented in Subsection 7.1.4 - trajectory with constant step. 57
45 The progress of the values of the objective functions used for trajectory tracking and heading control of particular robots in the experiment presented in Subsection 7.1.4 - trajectory with constant step. 58
46 The trajectory of the follower carrying the fill light in the experiment in simple environment with the obstacle. The arrows denote the heading of light at particular times t. 59
47 Control inputs used for controlling of the robots in the experiment with the obstacle presented in Subsection 7.1.4. 60
48 The progress of the values of the objective functions used for trajectory tracking and heading control of particular robots in the experiment with the obstacle presented in Subsection 7.1.4. 61

1 Introduction

The documentation of an interior part of large historical buildings in order to get the data for determination of the level of their damage is the well-known issue. In the past, it was necessary to build a costly scaffolding whenever restorers wanted to control the condition of paintings, statues or frescos in a copula of a church or other hardly accessible places. Since the sensors for autonomous data acquisition and methods for their processing have been already developed, restorers do not need to get into immediate proximity of scanned objects in person. Thanks to this fact, unmanned aerial vehicles (UAVs) equipped with these sensors, can be applied for the purpose of getting data from mentioned places.

However, hardly accessible places are often shaded and, in general, one UAV cannot film and light an object from the desired angle at the same time to be able to implement required lighting techniques. Therefore, we propose the method for autonomous stabilization of a formation of multi-rotor helicopters (marked as UAVs in this work) for the cooperative filming in dark conditions. The formation is made by one UAV, which is carrying a camera and other neighboring UAVs carrying light sources. The leader-follower approach and the model predictive control on receding horizon are used for formation driving and stabilization.

The presented method can be utilized for two lighting techniques commonly used by historians and filmmakers - Three point lighting and Strong side lighting. Three point lighting is a technique used in photography and video. The use of three separates lights enables photographers and filmmakers to reach almost any lighting setup including the control of shading and shadows on the scanned object. The strong side lighting is the restoration method which sets a light to a flat object in as small angle as possible. Such a way of illumination causes the shadows in the resulting image, due to a roughness and unevenness of the scanned surface. From these pictures, restorers are able to detect partly detached stucco in frescos or unproperly fixed tiles of mosaics.

We have verified the presented method by several simulations in Gazebo simulator under Robot Operating System (ROS). Afterwards, we also have deployed it in the real experiment, made with the multi-rotor helicopters of Multi-robot Systems Group at Department of Cybernetics, Faculty of Electrical Engineering (FEE), Czech Technical University in Prague (CTU).

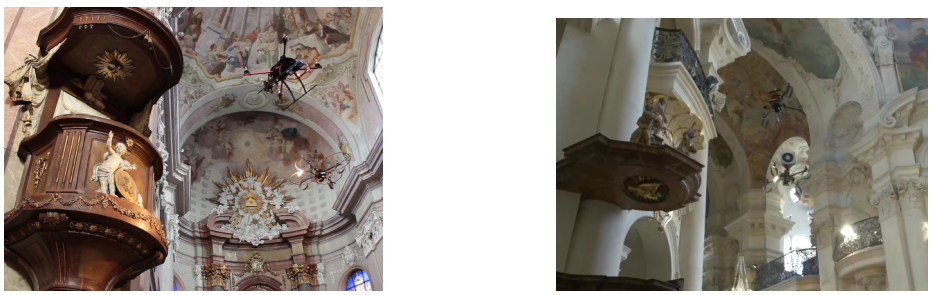

a) church in Sternberk **b)** st. Nicholas Church in Prague

Fig. 1 Deployment of the manually controlled quadrotors for filming. [1]

2 State of the art

Several methods using autonomous systems for documentation of cultural heritage sites were presented in recent years. They usually employ photogrammetry or laser scanners for getting 3D models of interiors or exteriors of the buildings. Mostly they are utilized to speed up the scanning process or to reach hardly accessible or even inaccessible places for people.

Static terrestrial laser scanners are used for acquiring point cloud data of the buildings in [2]. In [3] the long-range 3D laser scanner is employed for making the 3D model showing inter-relationship between indoor and outdoor profiles of the large temple. The handheld 3D mapping system called Zebedee is applied for capturing 3D model of the large outdoor area in [4]. This system enables efficient 3D mapping while an operator holding the device walks through the scanned environment. The level of autonomy is increased in [5], where the AVENUE, unmanned ground vehicle (UGV) equipped with the 3D laser scanner and system for autonomous view planning and data acquisition, is presented.

As the ground robots have limited operation space, the UAVs carrying cheap and lightweight cameras are often deployed for scanning of large buildings and environments [6], [7], [8]. Due to the unsatisfiable precision of Global Navigation Satelite Systems (GNSS) such as the Global Positioning System (GPS) inside of the buildings, the localization is one of the biggest problems of the robotic applications in the indoor environment. Although the methods for indoor localization were already explored by the robotic community [9] and [10], we have found only two works connected with documentation of cultural sites, where the method of the localization of the UAV is capable of working indoors. In [9] the simultaneous localization and mapping method is proposed, but it is verified only in the outdoor environment. The second one is the system with features that enables flying safe outdoor and indoor missions, which has been applied for scanning the statue in the cathedral. The proposed approach is designed for using in interiors of buildings thanks to the possibility of using the mutual UAV localization [11], [12] originally designed for control and stabilization of compact UAV swarms [13], [14], [15], [16].

We go much further beyond the works [6], [7], [8] in the way of data acquisition. Since the good light conditions play the key role in the quality of obtained images for their later processing, we propose the method for the formation of UAVs carrying a camera and lights. Moreover, our goal is not to make a system which has to be driven by the operator but to make the system capable of flying the assigned mission fully autonomously.

As regards the formation driving and stabilization, we apply the leader-follower approach together with the model predictive control, which are commonly used in the field of formation stabilization [17], [18], [19]. We take the benefit of long-term research of formation flying and stabilization within Multi-robot Systems group at FEE, CTU [20], [21], [22], [23], [24], [25], [26]. The aim of this project is to apply these results of basic research and to modify these approaches to satisfy the demands on the formation shape definition corresponding with the three point lighting scheme.

3 Problem definition

The problem solved in this work is to stabilize a formation of UAVs in the task of filming in dark conditions by a team of cooperative multi-rotor robots. One of these UAVs is carrying a camera (the leader), and other n_F robots (followers) are carrying light sources. All physical limitations of the robots and their parameters including a camera field of view and intensities of lights are known prior the mission. A shape of the formation is defined in the way, which corresponds to the design parameters of the three point lighting technique. It means that the desired position of the follower is defined with angles relative to the camera optical axis and the desired distance from the OoI.

In the proposed method, we assume a known map of an environment with a set of convex obstacles O. We do not presume an occurrence of dynamic obstacles excluding the other members of the formation, whose positions and planned trajectories are known to their neighbors. We also suppose that the UAVs are equipped with a system, providing the precise information about position of the robot in the given map. Due to expected applications of the presented method, this system has to be capable of working indoors. Some of the methods which fulfill this requirement are presented in chapter 2.

The other assumption is that the robots have a communication link for sharing their actual planned trajectories and alternatively (in the case of the availability of a precise global localization) the information about their actual positions with each other. It is essential for the application of the leader-follower approach and the collision avoidance within the formation.

Our aim is not to design a system, which is able to decide which objects should be scanned from which positions. This is a job of historians and document makers. Therefore, we assume that a plan of the mission is provided by the experts in the field of restorations or film industry. First of all, the given plan contains the desired trajectory of the leader. Each point on this trajectory is then labeled with a position of a corresponding observed object of interest (OoI). Additionally, a desired relative angles between the camera and the particular light sources together with a desired illuminance of OoI in each point of the trajectory are included in this plan.

Some of the presented assumptions are not necessary since the trajectory planning or online mapping methods were already explored and could be integrated into the proposed system. However, each of these features would add uncertainties in the entire system and so decreases its robustness, which is crucial for its deployment in real world applications.

4 Preliminaries

4.1 Model predictive control

Model Predictive Control (MPC) is the designation for control methods which explicitly use a model of the system to obtain control signal by minimizing an objective function. The model is used to predicate future behavior of the system for particular sequences of control inputs, and it is the base for computing the value of the objective function for these sequences. Therefore, the necessity of a good model together with higher computational demands are the biggest drawbacks of this methods. On the other hand, the easier development and maintenance in comparison to other advanced control methods, the relatively intuitive tuning, dealing with changing environment and suitability for multivariable control applications belong to their main advantages. For these strengths, they have a great utilization especially in refining, petrochemical and chemical industry and also in path planning and control of the robots [27].

In this work, we use the model predictive control concept for trajectory tracking for both leader and followers. Specifically, we apply the method, where a constrained finite horizon optimization is solved in time interval $\langle t_0, NT_s \rangle$, where t_0 is the time of current state, N is the number of so-called transition points, and T_s represents the sampling time between these points. A model of given system is then used for solving an optimization task defined as

$$U_j^* = \arg\min J(U_j), \;\; s.\, t.\; c(U_j) \leq 0, \tag{1}$$

where U_j is a sequence of control variables, $J(\cdot)$ denotes an objective function and $c(\cdot)$ represents a set of constraints. When a result of the optimization task U_j^* is obtained, first n values of the control sequence are applied for controlling the system and remaining $N - n$ values are together with the actual planned state taken as the initialization of the next optimization step (Fig. 2). These steps are then repeating until the end of the mission. This approach is presented in [28].

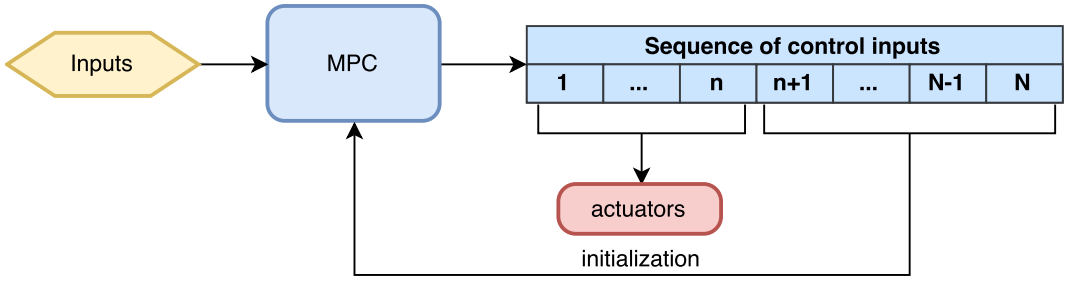

Fig. 2 The MPC concept, which is used for trajectory following in this work.

4.2 Configuration and parameters of robots

The configuration of the j-th robot in the formation is given by its position, heading, and orientation of camera (by leader) or light (by followers). The position $p_j(t)$ of the centre of the robot is defined with Cartesian coordinates $x_j(t)$, $y_j(t)$ and $z_j(t)$ in global coordinates system C. For simplification of description, the positions of camera and lights are supposed to be placed in the centre of the robot. The heading $\theta_j(t)$ is related to a kinematic model, which is presented in Section 4.3. The orientation of the camera and the light sources is defined by angles $\varphi_j(t)$ and $\xi_j(t)$, where $\varphi_j(t)$ stands for the angle from the x-axis in xy-plane of C and the $\xi_j(t)$ denotes the angle from the xy-plane in C.

We consider two types of parameters of the robots. The first group is made by those, which are linked to constraints on their motion. We will deal with them lately in this work. Apart from them, the parameters of the employed camera and light sources also have to be considered in this task.

The only important attribute of the camera, which influences the formation driving, is its field of view (FOV). It can be specified with two angles in the case of cameras with the rectangular shape of FOV - the horizontal angle of view AoV_h and the vertical angle of view AoV_v (Fig. 3).

Since our intention was not to design the best light setting, we do not deal with all parameters of lights including its precise attenuation. The only parameter which we use is the luminous intensity of the light of the j-th follower I_j. It is essential for calculation of desired distance between the follower and the OoI in the case that this distance is not given by experts, which is the preferred variant. We use the simplified model of the attenuation and so the desired illuminance may not be precise.

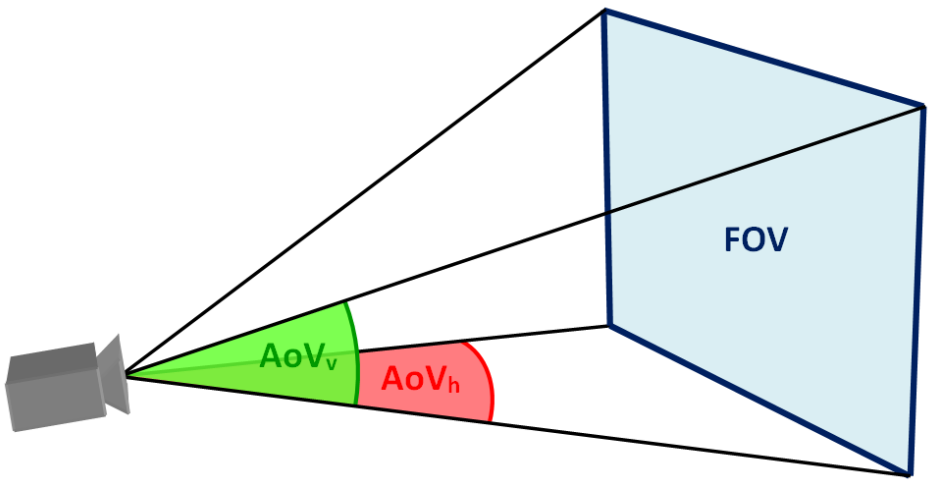

Fig. 3 Illustration of the horizontal angle of view AoV_h, the vertical angle of view AoV_v and the field of view FOV - the parameters of the camera.

4.3 Kinematic model

The kinematic model used in this work is described in this section. Since smooth trajectories are required for this application, we propose an UAV model, which is presented in [20]. It is inspired by standard car-like model with parameters velocity $v(t)$ and curvature $K(t)$, which is defined as

$$K(t) = \frac{\tan(\phi(t))}{L}, \tag{2}$$

where L is the distance between the front pair of wheels and rear pair of wheels, and $\phi(t)$ denotes the front steering angle. However, it adds the ascent velocity $w(t)$ to enable the change of altitude.

In the proposed method, we require controlling of the orientation of the camera and light sources. Therefore we extend this model with another two parameters, the angles $\varphi(t)$ and $\xi(t)$, which are controlled by angular velocities $\omega(t)$ and $\varepsilon(t)$. The independence of these parameters on the direction of the movement of the robot is essential for this method. In general, the UAVs are supposed to be equipped with the 2D gimbal for controlling the angle $\varphi(t)$ in range $\langle 0, 2\pi)$ and the angle $\xi(t)$ in range $(-\frac{\pi}{2}, \frac{\pi}{2})$. Nevertheless, the heading of UAVs is mostly independent of the direction of their movement, and some of them are able to stay in the air with desired orientation, so the method is applicable even without any use of gimbal.

The kinematic model of robot R_j, where $j \in \{L, 1, ..., n_F\}$, is given by equations

$$\begin{aligned}
\dot{x}_j(t) &= v_j(t)\cos(\theta_j(t)),\\
\dot{y}_j(t) &= v_j(t)\sin(\theta_j(t)),\\
\dot{z}_j(t) &= w_j(t),\\
\dot{\theta}_j(t) &= K_j(t)v_j(t),\\
\dot{\varphi}_j(t) &= \omega_j(t),\\
\dot{\xi}_j(t) &= \varepsilon_j(t).
\end{aligned} \tag{3}$$

As was mentioned in Section 4.1, we assume a constant time interval T_s between all transition points in receding horizon and constant control inputs $v_j(k)$, $K_j(k)$, $w_j(k)$, $\omega_j(k)$, $\varepsilon_j(k)$ between transition points with index k and $k+1$, $k \in \{0, 1, ..., N\}$ (the index $k = 0$ denotes the actual planned state). With this assumption we can get the following model for transition points by integrating equations (3) over the time interval T_s.

$$\begin{aligned}
x_j(k+1) &= \begin{cases} x_j(k) + \frac{1}{K_j(k+1)}[\sin(\theta_j(k) + K_j(k+1)v_j(k+1)T_s) - \\ -\sin(\theta_j(k))], \text{ if } K_j(k+1) \neq 0, \\ x_j(k) + v_j(k+1)\cos(\theta_j(k))T_s, \text{ if } K_j(k+1) = 0, \end{cases}\\
y_j(k+1) &= \begin{cases} y_j(k) - \frac{1}{K_j(k+1)}[\cos(\theta_j(k) + K_j(k+1)v_j(k+1)T_s) - \\ -\cos(\theta_j(k))], \text{ if } K_j(k+1) \neq 0, \\ y_j(k) + v_j(k+1)\cos(\theta_j(k))T_s, \text{ if } K_j(k+1) = 0, \end{cases}\\
z_j(k+1) &= z_j(k) + w_j(k+1)T_s,\\
\theta_j(k+1) &= \theta_j(k) + K_j(k+1)v_j(k+1)T_s,\\
\varphi_j(k+1) &= \varphi_j(k) + \omega_j(k+1)T_s,\\
\xi_j(k+1) &= \xi_j(k) + \varepsilon_j(k+1)T_s.
\end{aligned} \tag{4}$$

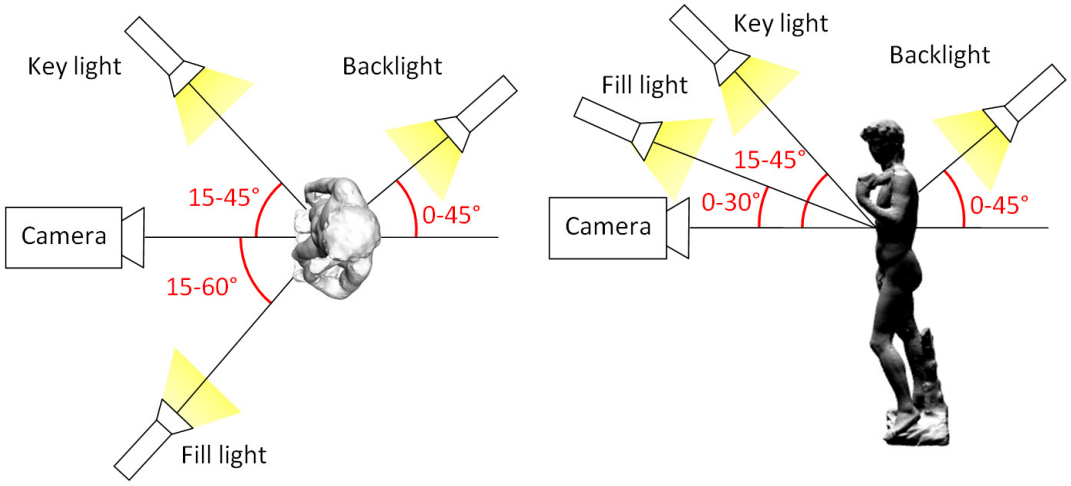

a) top view **b)** side view

Fig. 4 The common placement of lights in three point lighting technique.

4.4 Three point lighting

Three point lighting is a lighting technique, which is used for image rendering and lighting in video and photography. Its goal is to make scanned subjects look three-dimensional in a flat image, which is done with a use of the shading effects. The technique uses mostly three light sources, key light, fill light and backlight, for illuminating of the scanned object. However, the similar rules can also be applied in the case of one or two light sources. If we use less than three light sources, the light with the lowest importance for the particular application is omitted [29].

The dominant light in the three point lighting scheme is called the key light. It is the brightest one, which provides the main illumination of the object. The second light is referred to as the fill light, and it ensures illuminating of overshaded areas produced by the key light. Backlight, the third light source used in this technique, visually separates the filmed object from the background [30]. The common placement of lights in three point lighting technique is shown in Fig. 4.

The aim of this work is not to find the optimal placement of all lights in the three point lighting scheme, which is not a trivial problem. Thus we assume that the desired lighting angles, relative to the orientation of the camera, are known prior the mission. They are supposed to be given by filmmakers or restorers according to their knowledge, or the approach presented in [31], [30]. The method described in [29], which automatically computes the optimal light setting, is rather unusable for expected applications, because of its computational demands.

The possible applications of our method, which are described in Chapter 1, usually lead to film an object on the wall or in its nearness. In this case, it is clear that using backlight is impossible and so we use mostly only the key light and the fill light in our experiments. Nevertheless, the proposed method can be employed for the arbitrary number of followers with the little modifications, which are presented later in this work.

5 Formation stabilization

5.1 Leader-follower scheme

The leader-follower approach is used for the formation driving in this work. The desired trajectory of the leader together with the positions of Objects of Interest (OoIs) and angles between camera optical axis and lights are taken as the input of the task. The desired positions and light orientations of followers in time t depend on the camera orientation of the leader, given by angles $\varphi_L(t)$ and $\xi_L(t)$, and the position of actual scanned OoI $p_{OoI}(t) = \{x_{OoI}(t), y_{OoI}(t), z_{OoI}(t)\}$.

The position of the j-th follower and the orientation of its light are given by equations

$$\begin{aligned}
\varphi_j(t) &= \varphi_L(t) + \chi_j(t), \\
\xi_j(t) &= \xi_L(t) + \varrho_j(t), \\
x_j(t) &= x_{OoI}(t) - d_j \cos(\varphi_j(t)), \\
y_j(t) &= y_{OoI}(t) - d_j \sin(\varphi_j(t)), \\
z_j(t) &= z_{OoI}(t) + d_{xy}(t) \tan(\xi_j(t)),
\end{aligned} \tag{5}$$

where $d_{xy}(t)$ is defined as the euclidean distance omitting the z coordinate, $\chi_j(t)$ and $\varrho_j(t)$ are the relative angles of the j-th light related to the camera optical axis. $d_j(t)$ is the desired distance from the scanned object, which is given by experts or computed from desired illuminance $H(t)$ provided by the key light and the luminous intensity of the j-th light I_j in respect to equation

$$d_j(t) = \frac{-K_l + \sqrt{K_l^2 - 4K_q \left(-\frac{I_j}{\sigma_j H(t)} + K_c \right)}}{2K_q}. \tag{6}$$

The coefficient σ_j denotes the desired ratio between illuminance provided by the light of the j-th follower and the illuminance provided by the key light. The equation (6) is based on the model of attenuation $A(d_j(t))$,

$$A(d_j(t)) = \frac{1}{K_c + K_l d_j(t) + K_q d_j(t)^2}, \tag{7}$$

where K_c, K_l, K_q stand for the constant, linear and quadratic coefficients of light attenuation. The important assumption for usage of the equation (6) is that the lighted area $S = 1\,\mathrm{m}^2$ [32].

The usage of equations (5) is satisfying in the case of slow and small changes of $\varphi_L(t)$ and $\xi_L(t)$. If we consider the rotation of the leader around z-axis by up to π rad (which is common during the transition between two OoIs), it leads to unfeasible desired trajectories for followers. Therefore we adapt the calculating of $\varphi_j(t)$ and $\xi_j(t)$

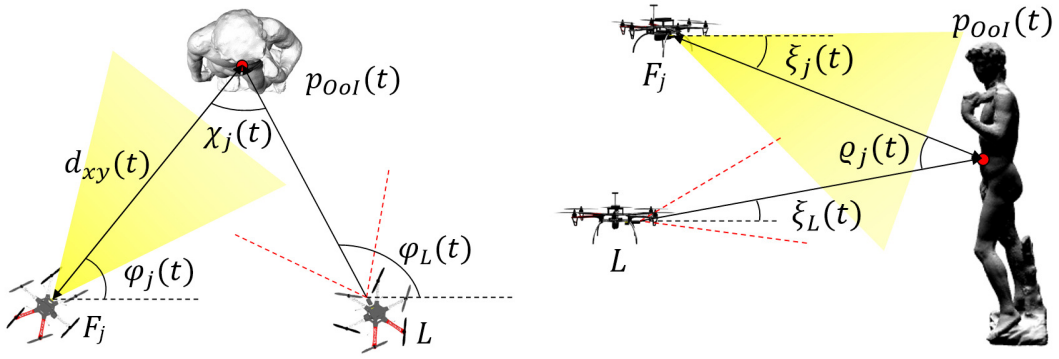

a) top view **b)** side view

Fig. 5 Illustration of the leader-follower scheme presented in this work.

in the following way

$$\varphi_j(t) = \begin{cases} \varphi_L(t) + \chi_j(t) & \text{if } |\varphi_L(t) - \text{ang}_h(p_L(t), p_{OoI}(t))| - \frac{AoV_h}{2} \leq 0, \\ \text{ang}_h(p_L(t), p_{OoI}(t)) + \chi_j(t) & \text{if } |\varphi_L(t) - \text{ang}_h(p_L(t), p_{OoI}(t))| - \frac{AoV_h}{2} > 0, \end{cases}$$

$$\xi_j(t) = \begin{cases} \xi_L(t) + \varrho_j(t) & \text{if } |\xi_L(t) - \text{ang}_v(p_L(t), p_{OoI}(t))| - \frac{AoV_v}{2} \leq 0, \\ \text{ang}_v(p_L(t), p_{OoI}(t)) + \varrho_j(t) & \text{if } |\xi_L(t) - \text{ang}_v(p_L(t), p_{OoI}(t))| - \frac{AoV_v}{2} > 0, \end{cases} \tag{8}$$

where the function $\text{ang}_h(\cdot)$ returns the angle between the vector defined by given points and the x-axis in the xy-plane and function $\text{ang}_v(\cdot)$ returns the angle between this vector and the xy-plane. Since the desired camera heading is always oriented towards the OoI, the $\varphi_j(t)$ and $\xi_j(t)$ are calculated from this heading in the case when the OoI is not in the camera field of view. In the opposite case, the actual planned heading is used for computing $\varphi_j(t)$ and $\xi_j(t)$, because the OoI should be illuminated from desired angles even if it is not in the centre of the shot. This approach ensures decreasing of both travelled distance during the mission and its dependence on the limitations on angular velocities $\varepsilon_L(t)$ and $\omega_L(t)$.

Let us note that our aim is not to define a desired shape of the formation, which should be held in the course of the mission. The presented computation of the position of the follower ensures that lighting of the OoI from desired distance and with desired relative angle to the camera optical axis is preferred to setting the lights to shine in a defined distance in front of the camera. The main disadvantage of this approach would be the fact, that the lights would face directly to the OoI only if it would be in the centre of the camera field of view. Thus the desired positions and orientations of the followers at times corresponding with particular transition points in control horizon are calculated according to equations (5) extended by equations (8). Described leader-follower scheme is illustrated in Fig. 5.

5.2 Scene capturing by leader with camera

Due to the fact that the control of the movement of the UAV is independent on its camera heading, two independent optimization problems are solved in this task. At first, an optimization problem for the position of the leader is solved, and its results are

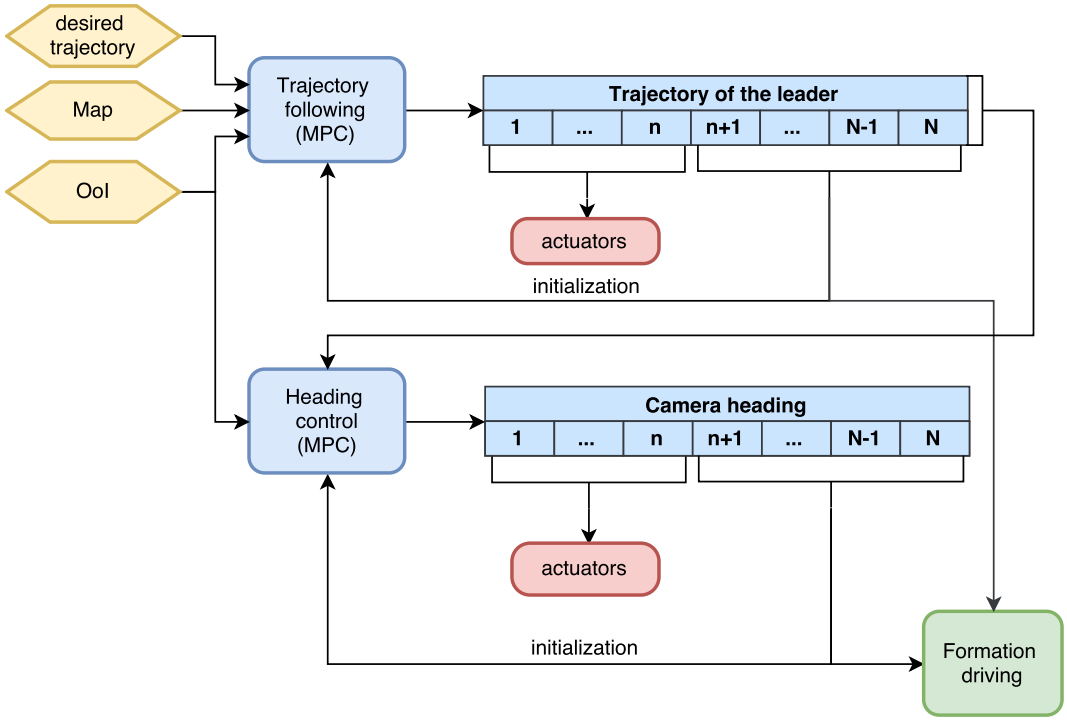

Fig. 6 The diagram of the part of the proposed system for formation stabilization which is connected with leader.

then used for computation of the desired camera heading in the second optimization task for camera heading control. The advantage of this separation is the reduction of the overall computational time needed for solving the task. The illustration of the part of the proposed system for formation stabilization which is connected with leader is shown in Fig. 6.

Let the $\psi_L(k) := \{p_L(k), \theta_L(k), \varphi_L(k), \xi_L(k)\}$ be the configuration of leader at k-th transition point in control horizon as described in Section 4.2 and let the $U_{L,1}(k) := \{v_L(k), w_L(k), K_L(k)\}$ and $U_{L,2}(k) := \{\omega_L(k), \varepsilon_L(k)\}$ be the sets of control inputs at k-th transition point in this horizon. For the purpose of optimization, we establish two independent vectors of decision variables. $\Omega_{L,1} := \{U_{L,1}(k)\}, k \in \{1, 2, ..., N\}$ stands for the control inputs connected with the position of the leader and $\Omega_{L,2} := \{U_{L,2}(k)\}, k \in \{1, 2, ..., N\}$ stands for the control inputs connected with the camera orientation. The trajectory, which is computed from the actual state and vectors of control inputs $\Omega_{L,1}$ and $\Omega_{L,2}$, is marked as Ψ_L in the description of the method.

5.2.1 Trajectory tracking

The trajectory tracking for the leader can be defined as an optimization task with a vector of decision variables $\Omega_{L,1}$ over the time horizon equal to NT_s, where N is the length of control horizon and T_s is the sampling time between transition points. Then the optimization problem can be described as a minimization of an objective function $J_{L,1}(\cdot)$ subject to a set of inequality constraints $g_o(\cdot)$, $g_f(\cdot)$ and $g_{N,1}(\cdot)$. It is

$$\begin{aligned} \Omega^*_{L,1} = \arg\min J_{L,1}(\Omega_{L,1}),\ s.\ t.\ g_o(\Psi_L, O) \leq 0, \\ g_f(\Psi_L, F) \leq 0, \\ g_{N,1}(U_{L,1}(k)) \leq 0, \forall k \in \{1, ..., N\}, \end{aligned} \tag{9}$$

where O is the set of all obstacles and F is the set of all followers in the formation.

Objective function for trajectory tracking

The form of the objective function for trajectory tracking is

$$\begin{aligned} J_{L,1}(\Omega_{L,1}) = \sum_{k=1}^{N} \Bigg[& \alpha ||p_{L,d}(k) - p_L(k)||^2 + \beta_1 (K_L(k-1) - K_L(k))^2 \\ & + \beta_2 (v_L(k-1) - v_L(k))^2 + \beta_3 (w_L(k-1) - w_L(k))^2 \\ & + \gamma \left(\min \left\{ 0, \min_{j \in \{1,\cdots,n_F\}} \left\{ \frac{||p_L(k) - p_j(0)|| - r_{s,r,L}}{||p_L(k) - p_j(0)|| - r_{a,r,L}} \right\} \right\} \right)^2 \\ & + \delta k \left(\min \left\{ 0, \frac{\mathrm{dist}(p_L(k), O) - r_{s,o}}{\mathrm{dist}(p_L(k), O) - r_{a,o}} \right\} \right)^2 \\ & + \eta \left(\min \left\{ 0, ||p(OoI) - p_{L,d}(k)|| - ||p(OoI) - p_L(k)|| \right\} \right)^2 \Bigg]. \end{aligned} \tag{10}$$

The first component penalises the deviations of the position of the leader $p_L(k)$, $\forall k \in \{1, ..., N\}$ from its desired position $p_{L,d}(k)$, $\forall k \in \{1, ..., N\}$. The second, the third and the fourth summand represent the differences in the sequence of curvatures $K_L(k)$, forward velocities $v_L(k)$ and ascent velocities $w_L(k)$, $\forall k \in \{1, ..., N\}$. So penalises fast changes of control inputs. $K_L(0)$, $v_L(0)$ and $w_L(0)$ denote the initial control inputs for particular optimization step.

In the fifth summation term, $r_{s,r,L}$ and $r_{a,r,L}$ are predefined safety radius of the leader, and its critical avoidance radius with respect to other robots in the formation. It guarantees the avoidance of other members of the formation, that are considered as obstacles. This term is significant in the case when some follower fails. Otherwise, the avoidance of followers is rather undesirable. Nevertheless, the reliable method how to recognize this failure does not exist and avoiding the right functional follower, which avoids leader itself, is preferred to the risk of the collision.

The function dist$(\cdot)$ returns the shortest Euclidean distance between its first and second argument. In this case, it means the distance between the position of the leader and the nearest obstacle in O. Thus the sixth component should provide the maximization of minimum distance from static obstacles, which appears within safety radius of the leader with respect to obstacles $r_{s,o}$. The form of the presented obstacle avoidance function is originally described in [33]. Its value is 0 when the nearest obstacle is outside the radius $r_{s,o}$ and it goes to infinity when the distance from nearest obstacle reaches the value of critical obstacle avoidance radius $r_{a,o}$. The multiplication by k gives greater importance to obstacles that are in safety radius closer to the end of the control horizon. It helps to prefer avoiding an obstacle to stop in front of it.

The last summand penalises solutions where the leader is further from the OoI than it would be if it goes exactly past the desired trajectory. It ensures that in situations in which there is an obstacle near the trajectory of the leader, the trajectory nearer to the OoI will be found. Therefore it helps to avoid situations in which the obstacle is just in front of the OoI from the point of view of the camera.

The values of coefficients α, β_1, β_2, β_3, γ, δ, η in equation (10) depend on particular applications. They serve to influence the demands on the found trajectory. For example with increasing values of β_i, $i \in \{1, 2, 3\}$ with respect to other coefficients smoother trajectories will be found, while with increasing values of γ and δ, safer trajectories will be found.

Constraint functions for trajectory tracking

The value of the constraint function $g_o(\cdot)$ for this optimization problem is defined as

$$g_o(\Psi_L, O) := r_{a,o} - \min\{\text{dist}(\Psi_L, O)\}. \tag{11}$$

The value of the constraint function $g_f(\cdot)$ is given by

$$g_f(\Psi_L, F) := r_{a,r,L} - \min_j\{\text{dist}(\Psi_L, F_j)\}, j \in \{1, ..., n_F\}, \tag{12}$$

where F_j is the particular robot from set F and n_F is the size of this set. This constraint has the similar meaning as the $g_o(\cdot)$, only the followers are considered as the obstacles in this case. Satisfying these two constraints ensures that the found solution will not lead to a collision with known obstacles or other members of the formation.

As was mentioned earlier, the vector of decision variables represents values of control inputs that will be used for the control of the robot. The movement capabilities of each robot depend on its design, so the constraint $g_{N,1}(\cdot)$ represents the limitation of control inputs. It is defined as

$$g_{N,1}(U_{L,1}(k)) := \begin{pmatrix} v_L(k) - v_{L,max} \\ v_{L,min} - v_L(k) \\ w_L(k) - w_{L,max} \\ w_{L,min} - w_L(k) \\ K_L(k) - K_{L,max} \\ K_{L,min} - K_L(k) \end{pmatrix}, \tag{13}$$

where $v_{L,max}$, $w_{L,max}$, $K_{L,max}$ are the upper bounds on particular control inputs of the leader and $v_{L,min}$, $w_{L,min}$ $K_{L,min}$ are the lower bounds on this inputs. These variables have to respect the physical limitations of deployed UAVs, but they may not be equal to them. Their absolute values can be decreased in order to guarantee slower motion of the leader.

5.2.2 Camera heading control

Since we required smooth and feasible changes of camera heading, we solve its control as an optimization task. As was mentioned earlier the camera heading control is independent of the trajectory tracking problem, and so it can be defined as an individual optimization task with a vector of decision variables $\Omega_{L,2}$ over the time horizon equal to NT_s. Then the optimization problem can be described as a minimization of an objective function $J_{L,2}(\cdot)$ subject to an inequality constraint $g_{N,2}(\cdot)$. It is given by

$$\Omega^*_{L,2} = \arg\min J_{L,2}(\Omega_{L,2}),\ s.\ t.\ g_{N,2}(U_{L,2}(k)) \leq 0, \forall k \in \{1, ..., N\}. \tag{14}$$

We use the result of optimization task for trajectory tracking $\Omega^*_{L,1}$ as the input for this optimization task because the desired camera heading depends on the planned trajectory of the leader.

Objective function for heading control

The objective function for heading control is given by

$$J_{L,2}(\Omega_{L,2}) = \sum_{k=1}^{N} \Big[\zeta_1(\mathrm{diff}_{ang}(\varphi_{L,d}(k), \varphi_L(k)))^2 + \zeta_2(\mathrm{diff}_{ang}(\xi_{L,d}(k), \xi_L(k)))^2 + \kappa_1(\omega_L(k-1) - \omega_L(k))^2 + \kappa_2(\varepsilon_L(k-1) - \varepsilon_L(k))^2\Big], \tag{15}$$

where the function $\mathrm{diff}_{ang}(\cdot)$ is defined as

$$diff_{ang}(\varphi_{L,d}, \varphi_L) = \begin{cases} \varphi_{L,d} - \varphi_L, & if \;\; \varphi_{L,d} - \varphi_L \leq \pi, \\ 2\pi - (\varphi_{L,d} - \varphi_L), & if \;\; \varphi_{L,d} - \varphi_L > \pi. \end{cases} \tag{16}$$

This function can be applied only if $\varphi_{L,d}, \varphi_L \in \langle 0, 2\pi)$.

The first two terms in equation (15) penalise the deviations of camera orientation, given by $\varphi_L(k)$ and $\xi_L(k)$, from its desired heading defined by angles $\varphi_{L,d}(k)$ and $\xi_{L,d}(k)$. These desired angles are calculated prior this optimization task from the known position of OoI and the actual planned trajectory computed from $\Omega^*_{L,1}$. The last two terms penalise fast changes in sequences of angular velocities $\omega_L(k)$ and $\varepsilon_L(k)$. The values of coefficients ζ_1, ζ_2, κ_1 and κ_2 influence the character of found solution. With increasing values of $\kappa_i, i \in \{1, 2\}$ with respect to values of $\zeta_i, i \in \{1, 2\}$, the solutions with the smoother course of angular velocities will be preferred to the minimization of deviations from desired heading and vice versa.

Constraint function for heading control

The only constraint function for heading control is $g_{N,2}(\cdot)$, which is defined as

$$g_{N,2}(U_{L,2}(k)) := \begin{pmatrix} \omega_L(k) - \omega_{L,max} \\ \omega_{L,min} - \omega_L(k) \\ \varepsilon_L(k) - \varepsilon_{L,max} \\ \varepsilon_{L,min} - \varepsilon_L(k) \end{pmatrix}, \tag{17}$$

where $\omega_{L,max}$, $\varepsilon_{L,max}$, $\omega_{L,min}$ and $\varepsilon_{L,min}$ are the upper respectively lower bounds on angular velocities $\omega_L(k)$ and $\varepsilon_L(k)$. They have to respect the physical limitations on deployed UAV, but as well as in the case of constraint function $g_{N,1}(\cdot)$, the limits may be more strict to slow down the rotation of the leader or its camera.

5.3 Scene lighting by followers holding the light

The desired paths of all followers are usually computed from a history of a path [34] of the leader or a history of its path and pre-planned path [28]. In comparison to these approaches, there is no pre-planned trajectory up to the target in this task. Since there is no guarantee that the trajectory given as the input is feasible and does not collide with obstacles, it is insufficient for computation of desired trajectories of followers. Therefore they have to be computed from the actual planned trajectory of the leader for next N transition points.

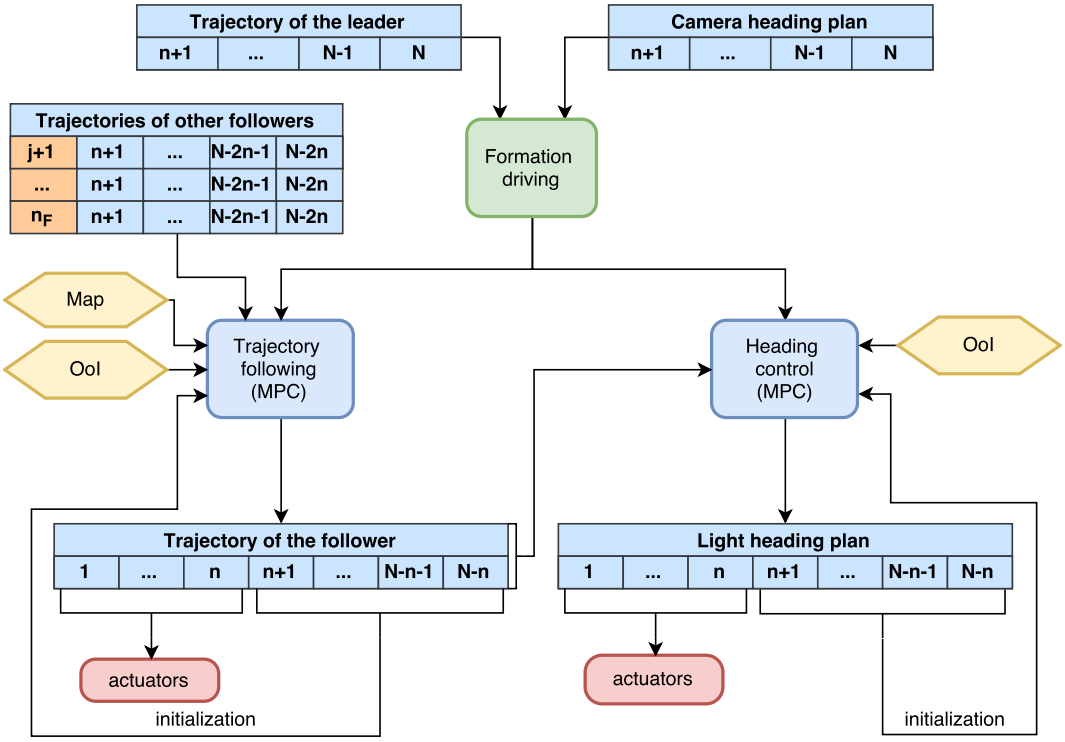

Fig. 7 The diagram of the part of the proposed system for formation stabilization, which is connected with followers. The process which precedes to the formation driving module is closer described in Fig. 6.

In the ideal case, the optimization tasks of all robots are solved subsequently in the same period of length nT_s. However, this approach leads to unreasonably high computational demands. For the purpose of their reduction, we use different lengths of control horizon for leader and followers and furthermore, we apply the index j as the indication of the rank of the robot within the formation.

It means that the length of the control horizon of the leader N is set to $N = N_F + n$, where N_F is the length of the control horizon of followers. Then the planned trajectory of the leader $\psi_L(i), i \in \{n+1, n+2, ...N\}$ is used for the computation of desired positions of followers for next N_F transition points, and the optimization tasks of leader and all followers can be solved parallelly. Setting the priority to followers is essential for application of collision avoidance function for planned trajectories. Since the followers plan their trajectories parallelly, the omission of this indication causes two-way avoidance, which leads to undesirable behaviour. The diagram illustrating the part of the proposed system for formation stabilization which is connected with followers is shown in Fig. 7.

Let the $\psi_j(k) := \{p_j(k), \theta_j(k), \varphi_j(k), \xi_j(k)\}$ be the configuration of the j-th follower at k-th transition point in control horizon as described in Section 4.2 and let the $U_{j,1}(k) := \{v_j(k), w_j(k), K_j(k)\}$ and $U_{j,2}(k) := \{\omega_j(k), \varepsilon_j(k)\}$ be the sets of control inputs at k-th transition point in this horizon. For the same reasons, which are described in Section 5.2, we devide the optimization problem in two seperate optimization tasks with vectors of decision variables $\Omega_{j,1} := \{U_{j,1}(k)\}, k \in \{1, 2, ..., N_F\}$ for the control inputs connected with the position of the follower and $\Omega_{j,2} := \{U_{j,2}(k)\}, k \in \{1, 2, ..., N_F\}$ for the control inputs connected with the orientation of its light. The trajectory of the j-th follower which is computed from its actual state and vectors of control inputs $\Omega_{j,1}$

and $\Omega_{j,2}$ is denoted as Ψ_j in following sections.

5.3.1 Trajectory tracking for followers holding the light

The trajectory tracking problem for the j-th follower can be defined as an optimization task with a vector of decision variables $\Omega_{j,1}$ over the time horizon equal to $N_F T_s$. Then it can be transformed into a minimization of an objective function $J_{j,1}$ subject to a set of inequality constraints $g_o(\cdot)$, $g_f(\cdot)$, $g_t(\cdot)$, $g_s(\cdot)$, and $g_{N,1}(\cdot)$. It is defined as

$$\begin{aligned}\Omega^*_{j,1} = \arg\min J_{j,1}(\Omega_{j,1}),\ s.\ t.\ & g_o(\Psi_j, O) \leq 0,\\ & g_f(\Psi_j, R) \leq 0,\\ & g_t(\Psi_j, \Psi_i) \leq 0, \forall i \in \{L, 1, ..., j-1\},\\ & g_s(\Psi_j, \Psi_L) \leq 0,\\ & g_{N,1}(k) \leq 0, \forall k \in \{1, ..., N_F\},\end{aligned} \tag{18}$$

where R denotes the set of all robots in the formation excluded the one whose trajectory is optimized.

Objective function for trajectory tracking

The objective function for the trajectory tracking of the j-th follower is given by

$$\begin{aligned}J_{j,1}(\Omega_{j,1}) = \sum_{k=1}^{N_F} \Bigg[& \mu ||p_{j,d}(k) - p_j(k)||^2 + \lambda_1 (K(k-1) - K(k))^2\\ & + \lambda_2 (v_j(k-1) - v_j(k))^2 + \lambda_3 (w_j(k-1) - w_j(k))^2\\ & + \nu \left(\min \left\{ 0, \min_{i \in \{L,1,\cdots,n_F\} \setminus j} \left\{ \frac{||p_j(k) - p_i(0)|| - r_{s,r,F}}{||p_j(k) - p_i(0)|| - r_{a,r,F}} \right\} \right\} \right)^2\\ & + \tau k \left(\min \left\{ 0, \frac{\text{dist}(p_j(k), O) - r_{s,o}}{\text{dist}(p_j(k), O) - r_{a,o}} \right\} \right)^2\\ & + \iota \left(\min \left\{ 0, \frac{\text{dist}_{ang}(p_L(k), p_j(k)) - d_{cs}}{\text{dist}_{ang}(p_L(k), p_j(k))} \right\} \right)^2 \Bigg]\\ & + \vartheta \Bigg(\sum_{k=1}^{N_F - n} \left(\min_{i \in \{L,1,\cdots,j-1\}} \left\{ 0, \frac{||p_j(k) - p_i(k+n)|| - r_{s,r,F}}{||p_j(k) - p_i(k+n)|| - r_{a,r,F}} \right\} \right)^2\\ & + \sum_{k=N_F-n+1}^{N_F} \left(\min \left\{ 0, \frac{||p_j(k) - p_L(k+n)|| - r_{s,r,F}}{||p_j(k) - p_L(k+n)|| - r_{a,r,F}} \right\} \right)^2 \Bigg),\end{aligned} \tag{19}$$

The first four and the sixth summand have the exactly same meaning as mentioned in Section 5.2.1. The fifth element is also similar to the one in equation (10). The only difference is that the safety radius of followers $r_{s,r,F}$ and their critical avoidance radius $r_{a,r,F}$ with respect to other robots in the formation are applied. As we have mentioned above, in general, the avoidance of followers is the undesirable behavior of the leader, but it is necessary if any of the followers fails. By setting the values $r_{s,r,F} > r_{s,r,L} + nT_s \max\{|v_{L,min}|, v_{L,max}\}$, we ensure that the value of the objective function $J_{j,1}(\cdot)$ will be influenced by the proximity of the leader sooner than the proximity of the j-th follower affects the value of the objective function $J_{L,1}(\cdot)$. Moreover, if we set the $r_{a,r,F} \geq r_{s,r,L} + nT_s \max\{|v_{L,min}|, v_{L,max}\}$, then the trajectory of the leader can be

influenced by right functional followers only in the case of changes in the surrounding environment.

The seventh term penalises the solutions where the j-th follower is closer to the border of the shot than d_{cs}. So d_{cs} denotes the minimum distance from the border of the shot which is supposed to be safe. The function that is used in this term has similar properties like the one for obstacle avoidance. The only difference is that the inappropriate distance from the border of the shot is set to 0.

The last element serves for penalising of solutions, which collide with trajectories of other robots in the formation. We suppose that the index j also stands for the priority of the robot in the hierarchy of the formation - the lower index, the higher priority. Then the followers should avoid only to trajectories of robots with higher priority. This approach enables to prefer the right position of key light before the right position of fill light, which is reasonable in proposed applications of this method.

The values of coefficients μ, $\lambda_i, i \in \{1, 2, 3\}$, ν, σ, τ and ι depend on particular applications similar as in the case of objective function $J_{L,1}$.

Constraint functions for trajectory tracking

The inequality constraint functions $g_o(\cdot)$, $g_f(\cdot)$ for this optimization problem are defined in a similar way as in Section 5.2.1, only the critical avoidance radius $r_{a,r,F}$ is used instead of the $r_{a,r,L}$. The constraint function $g_t(\cdot)$ is given by

$$g_t(\Psi_j, \Psi_i) := r_{a,r,F} - \min_k\{||p_j(k) - p_i(k)||\}, k \in \{1, ..., N\}, \tag{20}$$

The solutions, satisfying these constraints, are collision free with respect to trajectories of other robots with higher priority.

The constraint function $g_s(\cdot)$ is defined as

$$\begin{aligned} g_s(\Psi_j, \Psi_L) := -\min_k \max\{&\mathrm{diff}_{ang}(\mathrm{ang}_h(p_L(k), p_j(k)), \varphi_L(k)) - \frac{AoV_h}{2}, \\ &\mathrm{diff}_{ang}(\mathrm{ang}_v(p_L(k), p_j(k)), \xi_L(k)) - \frac{AoV_v}{2}\}, k \in \{1, ..., N\}. \end{aligned} \tag{21}$$

The function $\mathrm{ang}_h(A, B)$ returns the angle between the vector $\overrightarrow{AB}$ and the x-axis in the xy-plane and function $\mathrm{ang}_v(A, B)$ returns the angle between this vector and the xy-plane. Thus the value of function $g_s(\cdot)$ is greater than 0 if the solution leads to a trajectory, where the follower appears in the shot. Since some applications do not need to use the whole field of view, the border of the shot may not correspond with the parameters of the camera presented in Section 4.2. In this case, it is advantageous to set the values of AoV_h and AoV_v to conform the demands on the part of the scene which should not be disturbed by followers. Decreasing of their values leads to a wider range of feasible trajectories for followers. In extreme situation, this constraint can be omitted by setting $AoV_h = AoV_V = 0$.

As the bounds on control inputs of followers can be different from bounds on control

inputs of the leader, the inequality constraint $g_{N,1}(\cdot)$ is defined as

$$g_{N,1}(U_{j,1}(k)) := \begin{pmatrix} v_j(k) - v_{j,max} \\ v_{j,min} - v_j(k) \\ w_j(k) - w_{j,max} \\ w_{j,min} - w_j(k) \\ K_j(k) - K_{j,max} \\ K_{j,min} - K_j(k) \end{pmatrix}, \tag{22}$$

where $v_{j,max}$, $w_{j,max}$, $K_{j,max}$ are the upper bounds on particular control inputs of the follower and $v_{j,min}$, $w_{j,min}$ $K_{j,min}$ are their lower bounds. As in the case of the leader, these bounds have to respect the physical limitations of deployed robots. However, by setting lower bounds on their absolute values, the recognition of an unexpected behavior of the robots becomes easier. It is advantegous for safety pilots, who are supposed to be prepared to manually overtake the control of the robots in a case of their malfunction.

5.3.2 Light heading control

The problem of controlling heading of the light is similar to control of the camera heading, therefore we use similar approach as in Section 5.2.2. The control of the heading for the light of the j-th follower can be defined as an individual optimization task with a vector of decision variables $\Omega_{j,2}$ over the time horizon equal to NT_s. Then the optimization problem can be described as a minimization of an objective function $J_{j,2}$ subject to an inequality constraint $g_{N,2}(\cdot)$. It is given by

$$\Omega^*_{j,2} = \arg\min J_{j,2}(\Omega_{j,2}),\ s.\ t.\ g_{N,2}(U_{j,2}(k)) \leq 0, \forall k \in \{1, ..., N\}. \tag{23}$$

As in the case of the leader, we use the result of optimization task for trajectory tracking $\Omega^*_{j,1}$ as the input of this optimization task, because the desired heading of light depends on the planned trajectory of the j-th follower.

Objective function for heading control of follower

The objective function for heading control is defined as

$$\begin{aligned} J_{j,2}(\Omega_{j,2}) = \sum_{k=1}^{N} \Big[& \epsilon_1(\mathrm{diff}_{ang}(\varphi_{j,d}(k), \varphi_j(k)))^2 + \epsilon_2(\mathrm{diff}_{ang}(\xi_{j,d}(k), \xi_j(k)))^2 \\ & + \varsigma_1(\omega_j(k-1) - \omega_j(k))^2 + \varsigma_2(\varepsilon_j(k-1) - \varepsilon_j(k))^2 \Big], \end{aligned} \tag{24}$$

Particular terms of this function have the same meaning as in the equation (15), only the heading of lights is controlled instead of camera heading. ϵ_1, ϵ_2, ς_1 and ς_2 are coefficients, which serve to influence the character of found solution. for

Constraint function for heading control

The only constraint function for the heading control is $g_{N,2}(\cdot)$, which is defined as

$$g_{N,2}(U_{j,2}(k)) := \begin{pmatrix} \omega_j(k) - \omega_{j,max} \\ \omega_{j,min} - \omega_j(k) \\ \varepsilon_j(k) - \varepsilon_{j,max} \\ \varepsilon_{j,min} - \varepsilon_j(k) \end{pmatrix}, \tag{25}$$

where $\omega_{j,max}$, $\varepsilon_{j,max}$, $\omega_{j,min}$ and $\varepsilon_{j,min}$ are the upper respectively lower bounds on angular velocities ω_j and ε_j. They have to respect the physical limitations on deployed UAV, but as well as in the case of constraint function $g_{N,1}(\cdot)$, the limits may be stricter to slow down the rotation of the follower or its light.

5.4 Possible modifications and their advantages and disadvantages

We have also verified some approaches, which differs from the one which is described above. The first possible modification is based on the restriction on the motion of the robot. It is supposed that its altitude defined with $z_j(t)$ is constant during the whole mission. Thus the ascent velocity $w_j(t)$ and angular velocity $\varepsilon_j(t)$ are not included in the vectors of decision variables $\Omega_{j,1}$ and $\Omega_{j,2}$, which results in their shortening and reduction of time needed for solving the task. The comparison of computational demands of this "2D" method and the previously presented method is shown in Fig. 8.

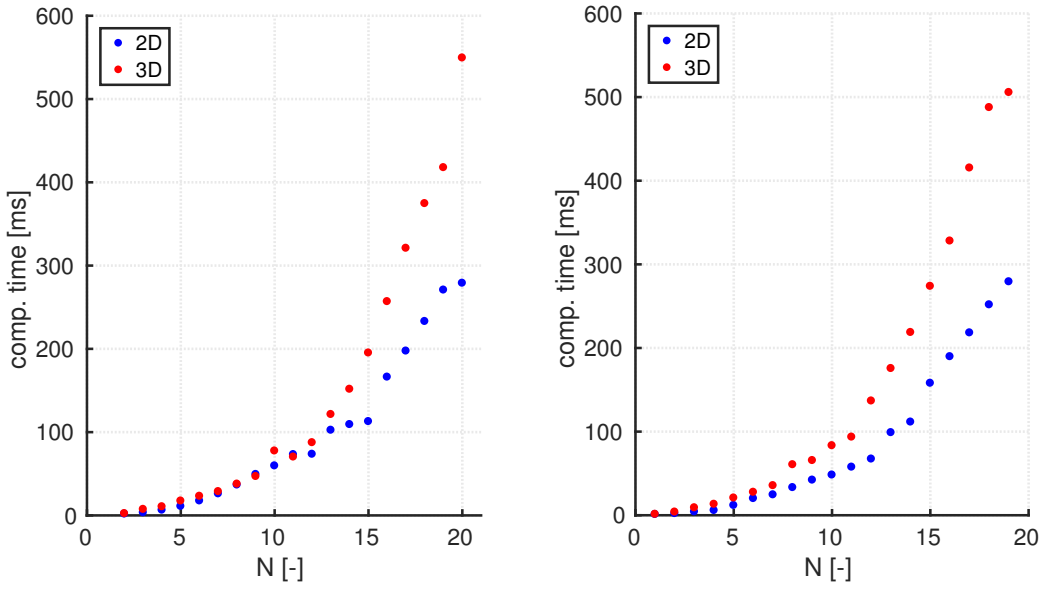

a) leader **b)** follower

Fig. 8 The influence of the length of control horizon N on the computational time of one step of the optimization process. Values for the "2D" method and the originally presented one (marked as "3D") are presented for comparison of their computational demands. Each value was obtained as the mean from 1000 runs of the algorithm.

This modification is useful in the case of unavailability of the gimbal mounted on UAVs or if we need to make the time of optimization lower. The main disadvantage is that reduction of the operational space of the robot leads to increase in the number of unfeasible trajectories. This drawback can be slightly improved by setting different desired altitudes to particular robots in the formation. If the differences in the altitudes are sufficient for collision avoidance of robots, it makes the computation of the objective function easier, and the constraints $g_f(\cdot)$ and $g_t(\cdot)$ can be dropped out. Nevertheless, the use of this method depends on the fact, whether the desired relative angles $\rho_j(t)$ and desired distances $d_j(t), j \in \{1, ..., n_F\}$, from OoI enable the safe differences among altitudes of all robots.

We propose another modification due to some applications, which prefers the illumination of the OoI from the desired angle to the shot free from followers. One way how to meet this requirement is to set the angles $AoV_h = AoV_v = 0$. With this approach, the follower's distance from the camera optical axis will be still penalised by the seventh component in equation (19). This is insufficient for some applications of back light. Therefore the constraint $g_s(\cdot)$ and the seventh summand in equation (19) can be completely omitted in these applications.

The last possible alteration of presented method, which we have tested, is to make the forward velocity of the leader constant. The benefit of this limitation is that it speeds up the optimization process thanks to the shortening of the vector of decision variables. Moreover, since the zero velocity is not allowed, it solves the problem with preferring stopping in front of the obstacle to going around it. However, the problem is in situations, in which the leader has to travel longer or shorter distance than was planned (due to obstacles etc.). Since it cannot change the forward velocity, it has to lengthen or shorten the remaining path in order to get closer to its desired position. Therefore it leads to significant deviations from the desired trajectory. In extreme situation when the shape of the desired trajectory is the segment, there is no way how to get closer to the desired position.

6 Implementation details

6.1 Sequential quadratic programming

The set of C functions called C Feasible Sequential Quadratic Programming (CFSQP) designed by Craig T. Lawrence, Jian L. Zhou, and André L. Tits, is used for solving the optimization problems in this work. It is the C code for solving constrained nonlinear optimization problems based on the Sequential Quadratic Programming (SQP), which is commonly used for solving the MPC problems. Its detailed description is given in [35]. This solver has been deployed in the project focused on control of multi-robot formation used for snow shoveling (previous work of Multi-robot Systems group). The implementation of the presented system is also based on this work.

6.2 Obstacle avoidance

Since our goal was not to find and integrate the best way, how to find the distance from the nearest obstacle in set O, we use only two basic shapes of obstacles within the implementation. Their top views are presented in Fig. 9 and we suppose that their heights are infinite. The reason for usage of these simple shapes is in the reduction of the computational time. However, the methods which are able to deal with any shape of the obstacle in reasonable time already exists and can be integrated into the presented system. For example, the distance from the nearest obstacle can be computed for each point in the segmented map prior the mission and saved in the hash-map. Then the values corresponding to particular points in the map can be read from the prepared hash-map during the optimization process. In this case, the computational time will not depend nor on the number of obstacles neither on their shape.

The shape of j-th robot as the obstacle is supposed to be the sphere with radius r_j, which is given by the distance between the centre of the robot and the most remote point on its construction.

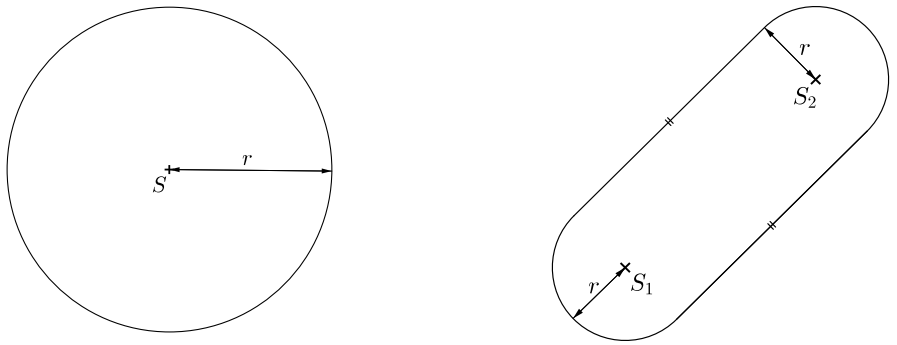

a) The first type of obstacle - circle defined by its centre and radius

b) The second type of obstacle defined by two points and the radius

Fig. 9 Two types of obstacles considered within the optimization task

7 Experimental results

The experimental results are presented in this section. Following units are used in all graphs: m for coordinates $x_j(t)$, $y_j(t)$ and $z_j(t)$, rad for angles $\varphi_j(t)$ and $\xi_j(t)$, $m\,s^{-1}$ for velocities $v_j(t)$ and $w_j(t)$, m^{-1} for curvature $K_j(t)$, and $rad\,s^{-1}$ for angular velocities $\omega_j(t)$ and $\varepsilon_j(t)$. For the more transparent description of formation settings, we present the desired distances $d_j(t)$ instead of the values $H(t)$, I_j and coefficients of attenuations, which define this distance. Since we suppose the constant value of $H(t)$ in all experiments we present the distance $d_j(t)$ as the constant in following subsections. All values of objective functions are normalized by $\frac{1}{N}$ in the case of leader and by $\frac{1}{N_F}$ in the case of follower. It allows their better comparison in the case of the changing length of the horizon.

7.1 Simulation

All of the presented simulations were realized in Gazebo simulator under the Robot Operating System (ROS) with the usage of the system of controllers designed by Multi-robotic Systems Group at Department of Cybernetics at FEE, CTU. The maps, in which we have tested the system, are inspired by historical buildings or by the expected environment for real experiment. The source of models used in the simulations is the open database *thinginverse.com*.

7.1.1 Experiment in complex environment

The experiment made with six OoIs and fourteen obstacles including walls and the OoIs is presented in this subsection. The software of the simulator in which we have tested the system does not allow to control the angle $\varphi_j(t)$ independently of the heading of the UAVs. Moreover, the camera is fixed on the frame of the robot and so it does not allow to control camera heading independently of the heading of the UAV at all. Since the modification of the simulator is beyond the goals of this work and its actual version is sufficient for the verification of the proposed system, we use the following setting. The followers are equipped with the gimbals for controlling the angle $\xi_j(t)$ and the angle $\varphi_j(t)$ is controlled by changing the heading of the particular UAV. The camera is fixed on the frame of the leader, and therefore we can control only the $\varphi_L(t)$ angle in the same way as in the case of followers. This experiment verifies several functions of the proposed approach: obstacle avoidance, smooth transition between two objects of interest and avoidance of collision with other robots in the formation.

Constants used in this experiment are described in Tables 1, 2. The reason for setting the smaller values to coefficients connected with the penalisation of fast changes in the sequence of control inputs in comparison to others, is that we prefer the smaller deviations from desired positions to less aggressive control inputs. Due to expected applications of the proposed system, the limitations on control inputs presented in Table 3 are strict. So they sufficiently limit the forward, ascent, and angular acceleration. The bounds on the velocity $v_L(t)$ do not involve the zero velocity. It helps to obstacle avoidance because it does not allow to find a solutions that stop in front of the obstacle.

α [−]	β_1 [−]	β_2 [−]	β_3 [−]	γ [−]	δ [−]	N [−]	$r_{s,o}$ [m]	$r_{s,r,L}$ [m]	AoV_h [rad]
1	0.1	0.1	0.1	0.2	0.5	13	2.5	2.5	1.85
η [−]	ζ_1 [−]	ζ_2 [−]	κ_1 [−]	κ_2 [−]	T_s [s]	n [−]	$r_{a,o}$ [m]	$r_{a,r,L}$ [m]	AoV_v [rad]
0.5	1	1	0.01	0.01	0.4	1	1.5	1.5	1.57

Tab. 1 The constants used in the optimization task of the leader in the experiment presented in Subsection 7.1.1.

μ [−]	λ_1 [−]	λ_2 [−]	λ_3 [−]	ν [−]	τ [−]	d_{cs} [m]	N_F [−]	$r_{s,o}$ [m]	$r_{s,r,F}$ [m]	d_1 [m]	σ_1 [−]
1	0.2	0.2	0.4	1	2	2	12	2.5	3.5	7.25	1
ι [−]	ϑ [−]	ϵ_1 [−]	ϵ_2 [−]	ς_1 [−]	ς_2 [−]	T_s [s]	n [−]	$r_{a,o}$ [m]	$r_{a,r,F}$ [m]	d_2 [m]	σ_2 [−]
2	1	1	1	0.05	0.05	0.4	1	1.5	2.5	7.45	0.7

Tab. 2 The constants used in optimization task of the followers in the experiment presented in Subsection 7.1.1.

j	L - leader	1 - key light	2 - fill light
$v_{j,min}[\mathrm{m\,s^{-1}}]$	0.08	−0.60	−0.60
$v_{j,max}[\mathrm{m\,s^{-1}}]$	0.50	0.60	0.60
$K_{j,min}[m^{-1}]$	−2.00	−2.00	−2.00
$K_{j,max}[m^{-1}]$	2.00	2.00	2.00
$w_{j,min}[\mathrm{m\,s^{-1}}]$	−0.50	−0.60	−0.60
$w_{j,max}[\mathrm{m\,s^{-1}}]$	0.50	0.60	0.60
$\omega_{j,min}[\mathrm{rad\,s^{-1}}]$	−0.10	−0.25	−0.25
$\omega_{j,max}[\mathrm{rad\,s^{-1}}]$	0.10	0.25	0.25
$\varepsilon_{j,min}[\mathrm{rad\,s^{-1}}]$	−0.20	−0.25	−0.25
$\varepsilon_{j,max}[\mathrm{rad\,s^{-1}}]$	0.20	0.25	0.25

Tab. 3 The limitations on control inputs used in the experiment presented in Subsection 7.1.1.

At the start of the mission, the formation scans the statue, which is lighted by followers with relative angles $\chi_1(t) = 0.754\,\mathrm{rad}$, $\varrho_1(t) = 0.2\,\mathrm{rad}$ for the follower with the key light and $\chi_2(t) = -0.754\,\mathrm{rad}$, $\varrho_1(t) = -0.1\,\mathrm{rad}$ for the follower with the fill light. These values correspond with the three point lighting method and thus ensure better 3D-perception of the scanned OoI in the resulting image. Since the values $d_j(t), j \in \{1, 2\}$ are constant within scanning of one OoI, the trajectory of j-th follower is the part of the circle with radius $d_j(t)$. The trajectory of the leader is also the part of the circle with constant radius, and so the formation holds the same shape while scanning the first OoI until it has to avoid the obstacle.

The second OoI is a flat image, so during the first transition between the OoIs also

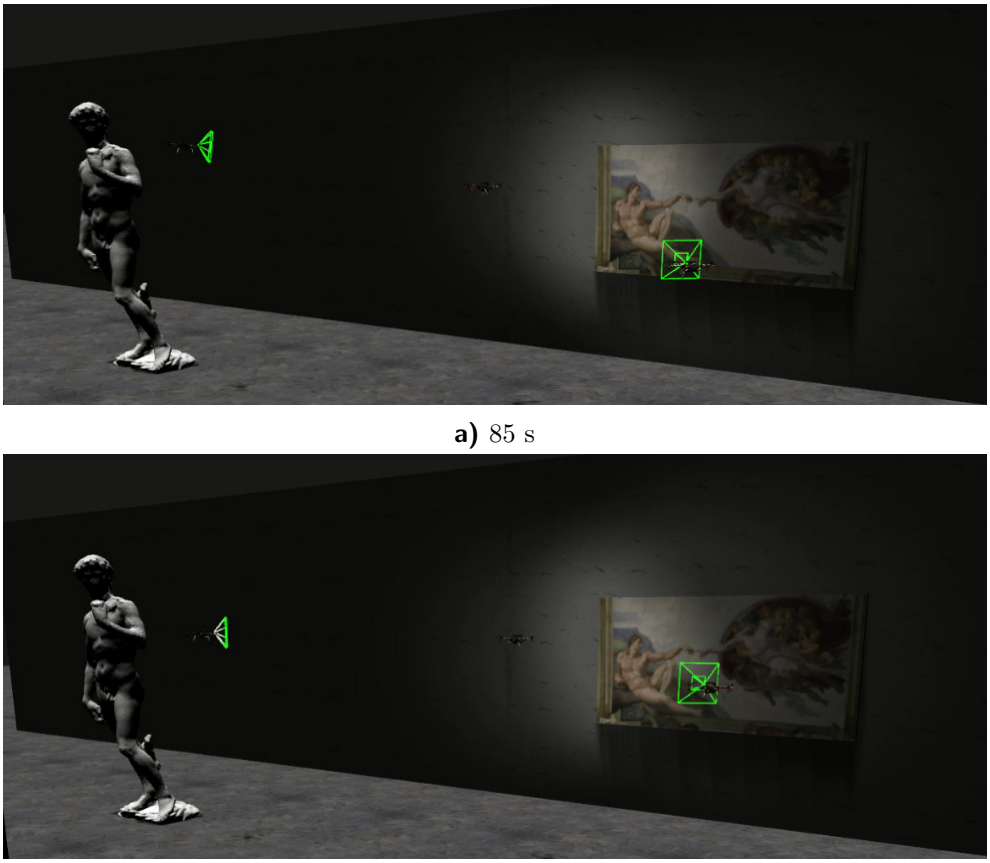

a) 85 s

b) 88 s

Fig. 10 Snapshots of the formation during the change of light angles because of the transition between lighting of the 3D and 2D image. The changes of the vertical lighting angles $\varrho_j(t)$ are accompanied by the change of the altitude of both followers.

the desired angles $\varrho_1(t)$ and $\varrho_2(t)$ are changed. In the case of a lighting of a 2D image, a 3D-look is unnecessary, and so the lighting with relative angles $\varrho_j(t) = \chi_j(t) = 0\,\text{rad}, j \in \{1, 2\}$ is sufficient. However, we use $\chi_1(t) = 0.754\,\text{rad}$, $\chi_2(t) = -0.754\,\text{rad}$ to avoid lighting beyond the leader and set the desired position of the followers into the critical avoidance radius of the leader $r_{a,r,L}$. The change of the desired angles $\varrho_1(t)$ and $\varrho_2(t)$ is illustrated in Fig. 10.

The third and the fourth OoI are also flat, and so all relative light angles are the same as in the previous part of the trajectory. Each transition between the OoIs results in the rise of the values of the objective functions $J_{j,1}, j \in \{1, 2\}$ and $J_{j,2}, j \in \{L, 1, 2\}$, which are presented in Fig. 11. The value of the objective function $J_{L,1}$ is not influenced by the transitions because the desired position of the leader does not depend on the position of currently scanned OoI. Since the desired position of the follower is computed from the position of OoI $p_{OoI}(t)$ and the angle $\varphi_L(t)$ or the position $p_L(t)$ (see equation (8)), the switch between OoIs influences the values of both objective functions of followers.

The fourth transition between the flat image and the 3D statue is again accompanied by the change of the relative light angles to $\varrho_1(t) = 0.2\,\text{rad}$ and $\varrho_2(t) = -0.1\,\text{rad}$. During this transition, the follower with the fill light turns around its axis counter-clockwise, which is not ideal. However, it is an expected behavior. Due to the limited length of the control horizon, the final desired heading does not influence the value of the objective function at the time of the start of the transition. So the actual position of the follower

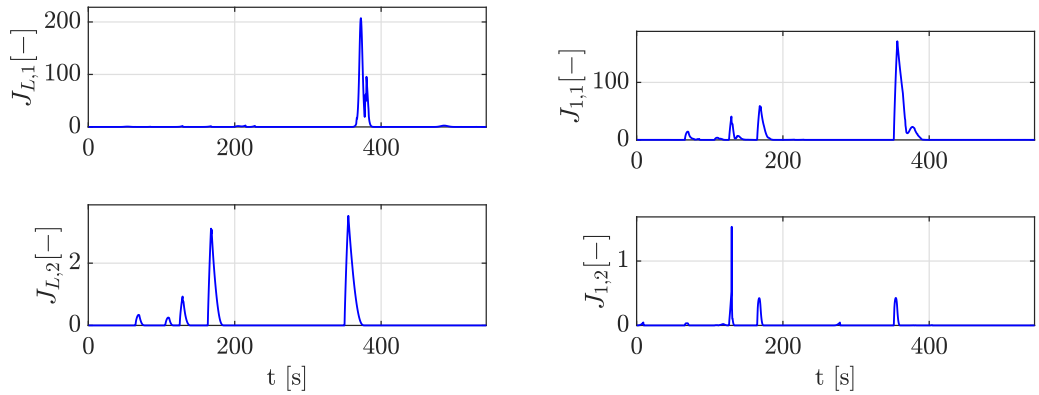

a) leader carrying the camera

b) follower carrying the key light

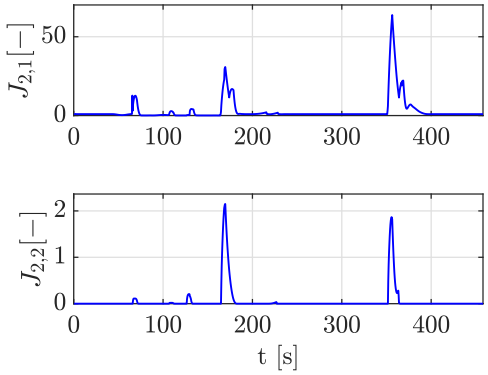

c) follower carrying the fill light

Fig. 11 The progress of the values of the objective functions used for trajectory tracking and heading control of particular robots in the experiment presented in Subsection 7.1.1.

at this time results in the desired heading that is closer to the actual heading in the case of turning counter-clockwise. This transition is also influenced by the modification of equations for computing position of the follower (equation (8)). The whole transition is shown in the sequence of snapshots in Fig. 12.

The next interesting part of the mission is the flight through the narrow corridor. From trajectories which are shown in Fig. 14, 15 and 16 is evident that the followers use the change of altitude to avoid collision with other robots in the formation and also to avoid the presence of the follower in the shot. The control inputs used for controlling of the leader and both followers are shown in Fig. 13. The experiment is captured in the video: `https://youtu.be/OcDyQFgTjcs`, which is also located on the enclosed CD.

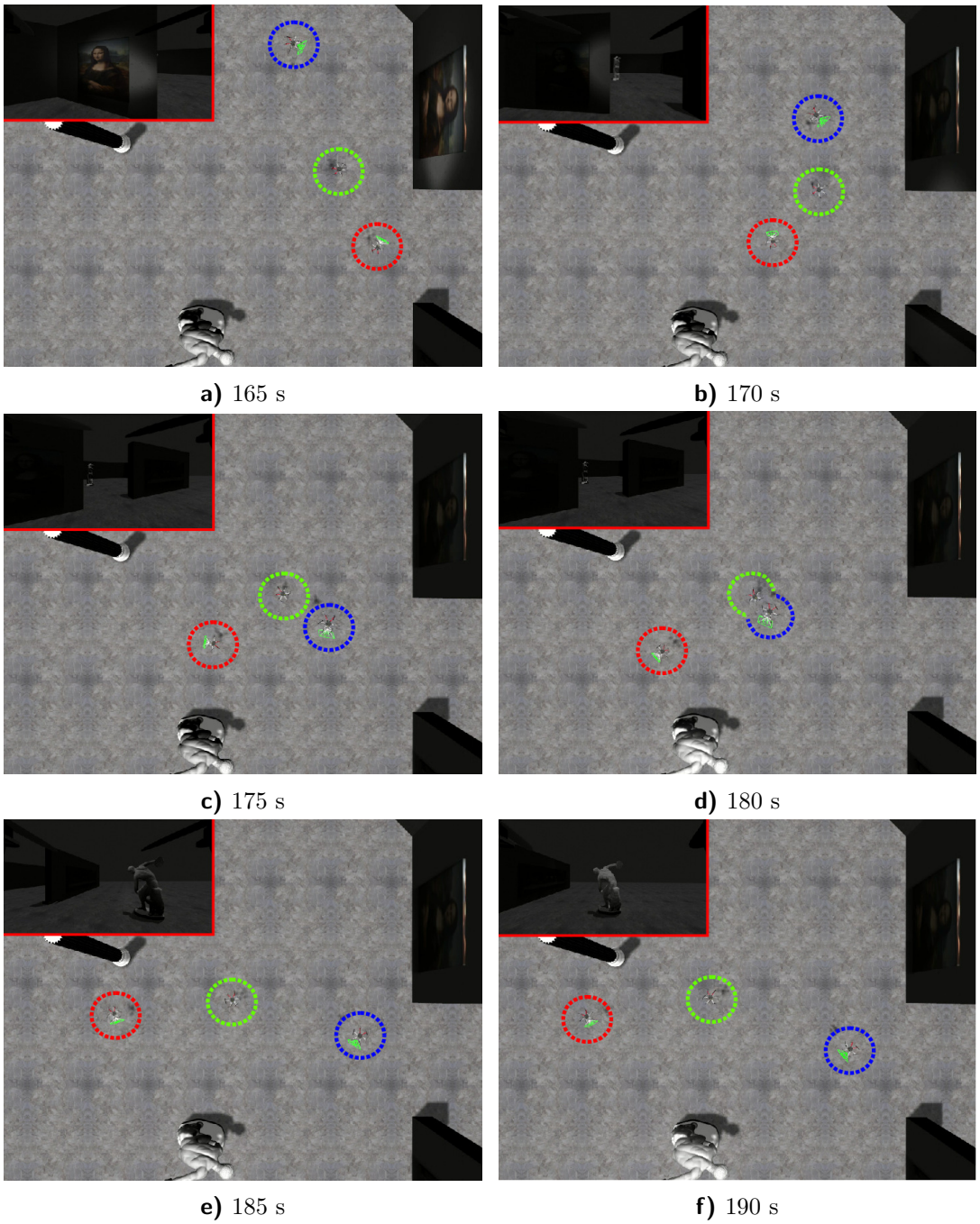

a) 165 s **b)** 170 s **c)** 175 s **d)** 180 s **e)** 185 s **f)** 190 s

Fig. 12 Snapshots of the formation during the transition to another object of interest. The followers use the change of the altitude for avoiding other robots in the formation and the presence in the FOV (in the case of followers). It is more evident from Fig. 15, 16 or the video: `https://youtu.be/OcDyQFgTjcs`.

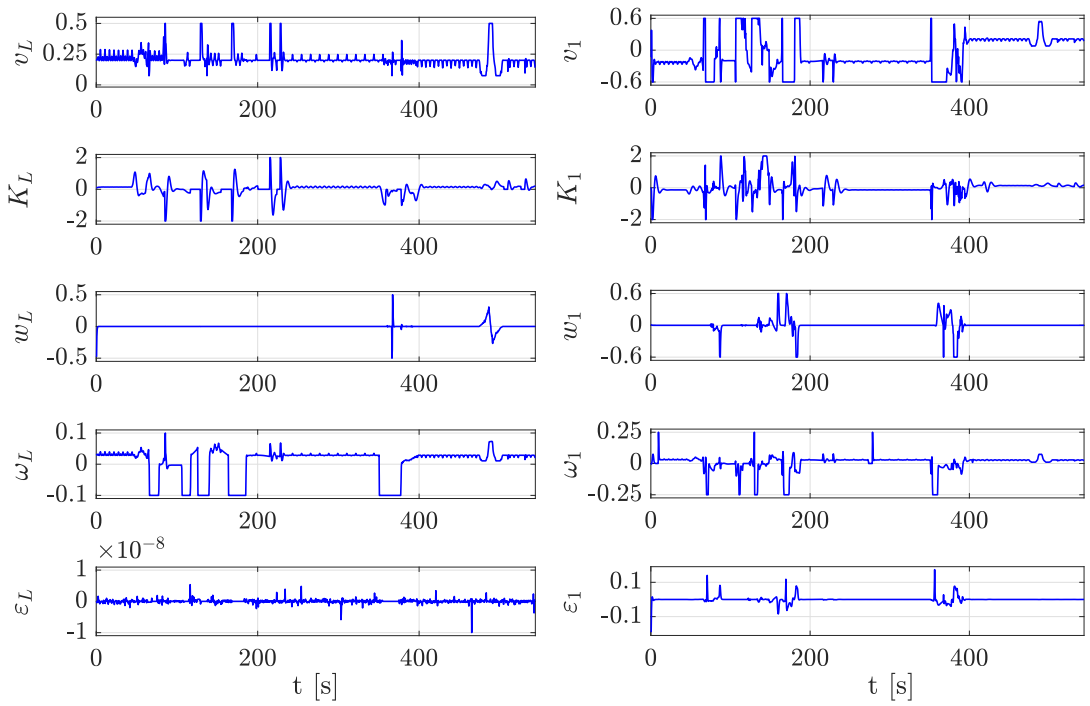

a) leader with camera **b)** follower with key light

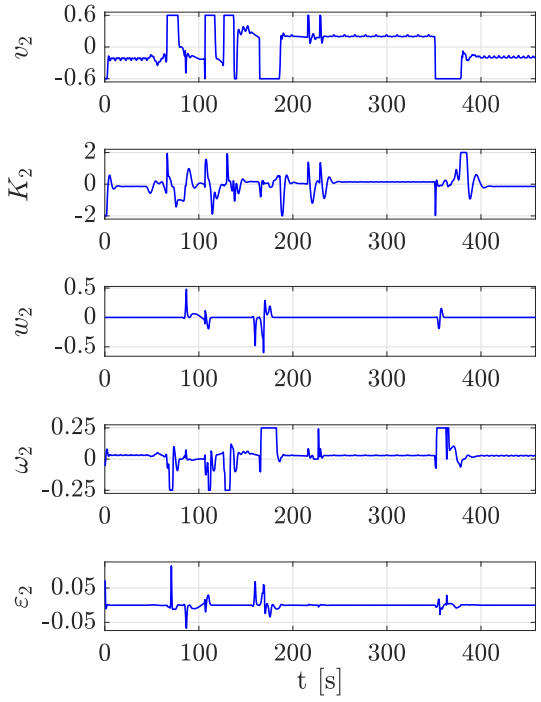

c) follower with fill light

Fig. 13 Control inputs used for controlling of the robots in the experiment presented in Subsection 7.1.1.

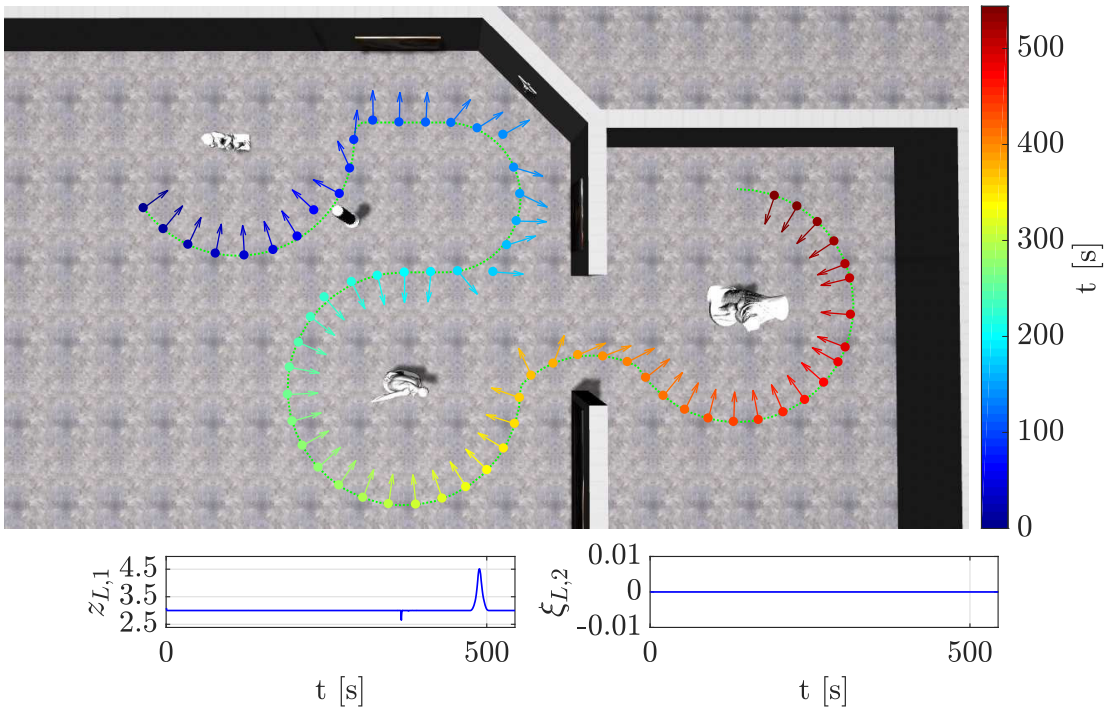

Fig. 14 The trajectory of the leader in the experiment in the complex environment. The arrows denote the heading of the camera at particular times t, and the green dotted line shows the desired trajectory.

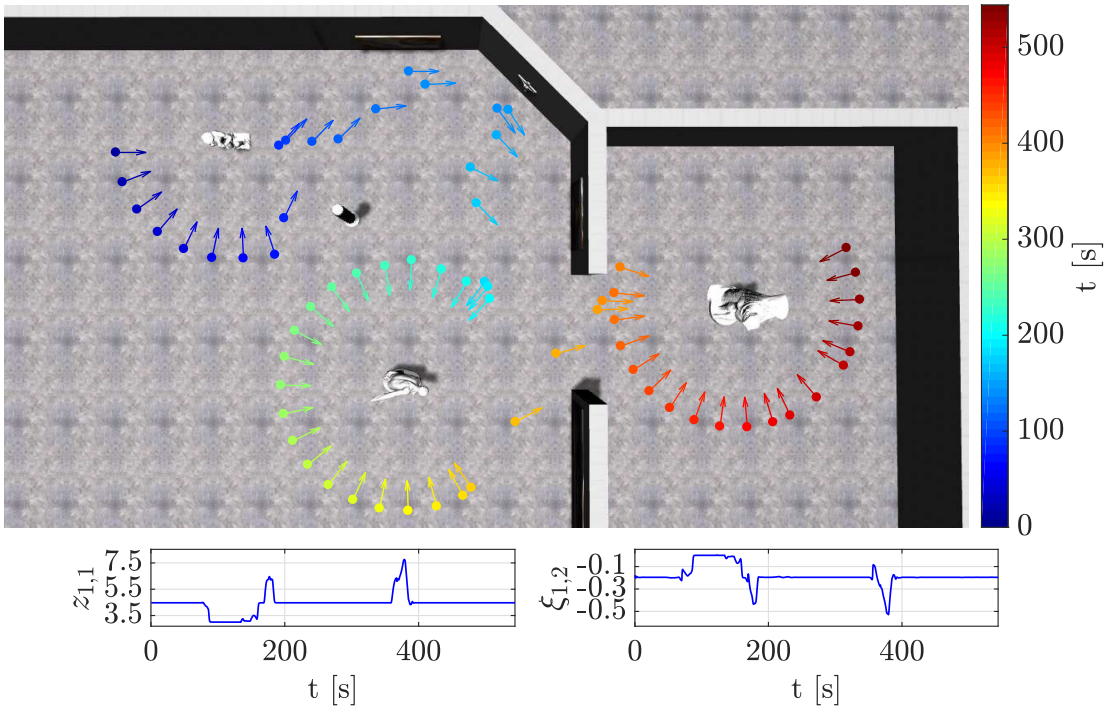

Fig. 15 The trajectory of the follower carrying the key light in the experiment in the complex environment. The arrows denote the heading of the light at particular times t.

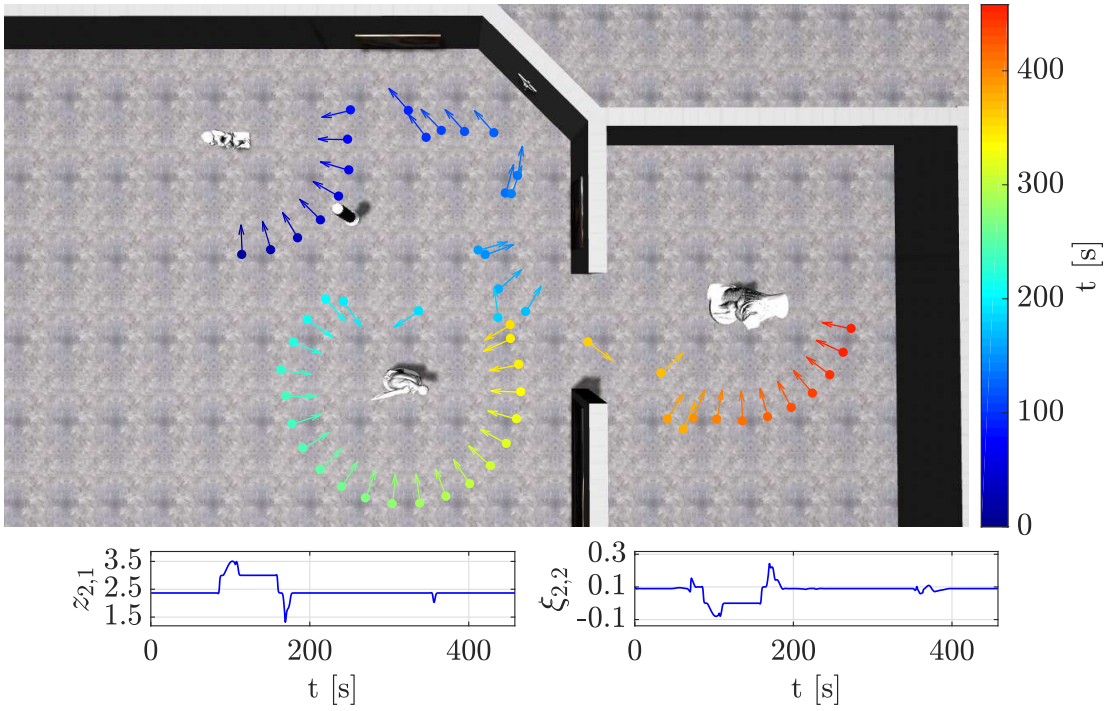

Fig. 16 The trajectory of the follower carrying the fill light in the experiment in the complex environment. The arrows denote the heading of the light at particular times t.

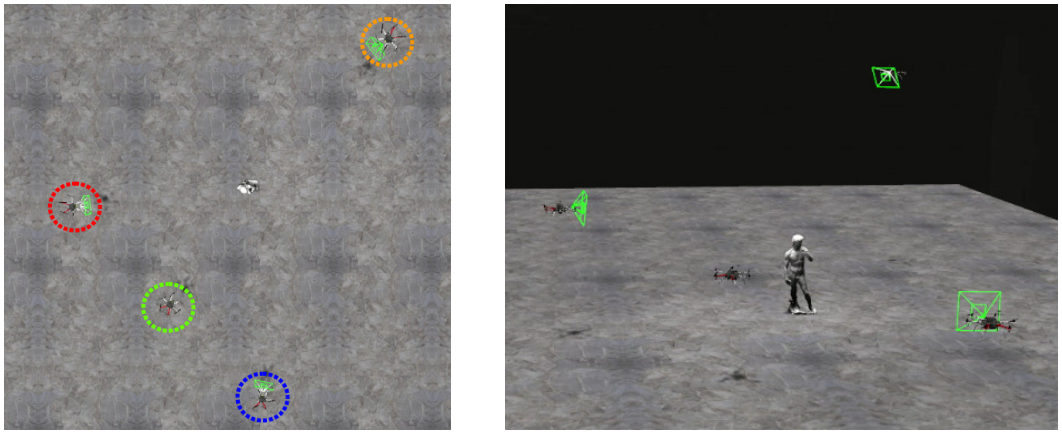

a) top view **b)** side view

Fig. 17 Snapshot of the formation with three lights during the scanning of the OoI. The dotted circles highlight the leader (green), the follower provided the key light (blue), the follower provided the fill light (red), and the follower provided the backlight (orange).

7.1.2 Experiment with three lights

In this experiment, we have verified the system in a simple environment with two statues, which is feasible also for the deployment of the backlight. It means that all OoIs are at a sufficient distance from the walls, and so they can be lighted from any side. We set the value of $AoV_v = 0.1\,\text{rad}$ for the follower carrying the backlight, and thus enables flying within real FOV to this follower. For the illustration of the shape of the formation during scanning one OoI see Fig. 17. The trajectory of the leader is illustrated in Fig. 18. The trajectories of the followers (Fig. 28, 29, 19), the constants (Tables 5, 6), the limitations on control inputs (Table 7), graphs of the control inputs used for controlling of the robots (Fig. 30), and graphs of the progress of the objective functions (Fig. 31) in the experiment with three lights are presented in Appendix B. The experiment is captured in the video: `https://youtu.be/Dg9FrjpV8-g` , which is also located on the enclosed CD.

7.1.3 2D-modification - two rooms environment

We have also verified the 2D-modification, which is presented in Section 5.4. As we have already mentioned, it is useful especially when the gimbal is unavailable or cannot be mounted on the affordable robots. The trajectory of the leader is shown in Fig. 20. Other trajectories (Fig. 32, 33), the constants (Tables 8, 9), the limitations on control inputs (Table 10), graphs of the progress of the objective functions (Fig. 35), and the graphs of the control inputs used for controlling of the robots (Fig. 34) are presented in Appendix B. The video (`https://youtu.be/jpJzaMv0G8s`), which is also located on the enclosed CD provides the better illustration of the experiment.

The sequence of snapshots presenting the transition between two OoIs and concurrent fly by the narrow corridor is shown in Fig. 21. It presents the advantage of our approach, which does not prefer to hold the shape of the formation during the whole mission. In this situation, holding the desired shape without a trajectory planning for the entire formation would lead to an unfeasible trajectory for the follower carrying the fill light. The experiment also shows the drawback of the 2D-approach in comparison to the original one presented in the experiment in Section 7.1.1. Due to the unavailability of changing the altitude, the follower has to wait in front of the corridor until the leader

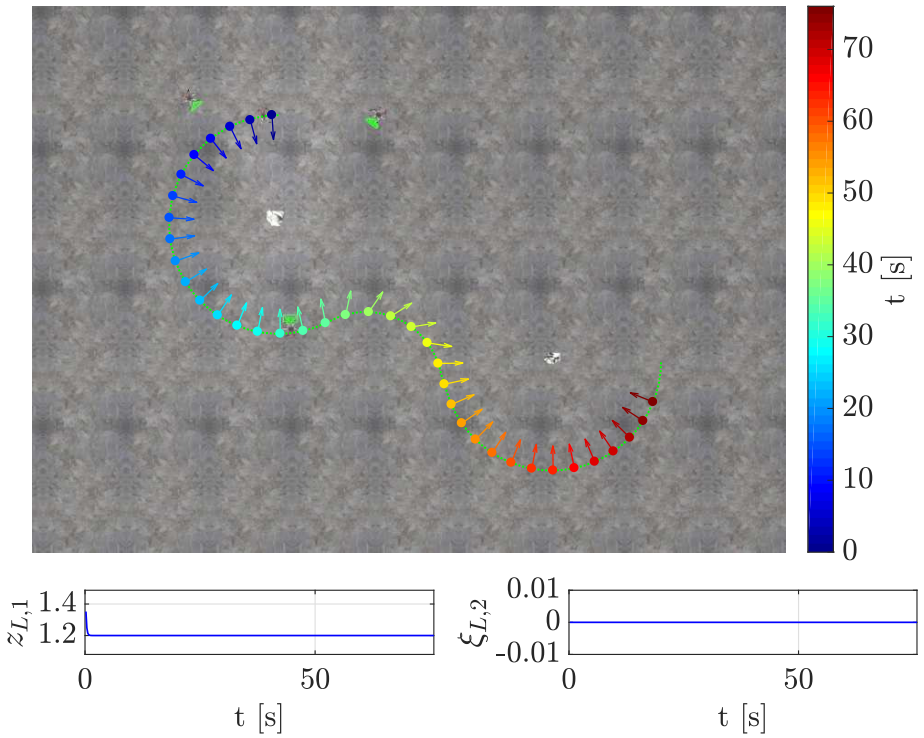

Fig. 18 The trajectory of the leader in the experiment with three lights. The arrows denote the heading of the camera at particular times t, and the green dotted line shows the desired trajectory. The trajectories of the followers in this experiment are presented in Fig. 19, 29, 28 in the appendix B.

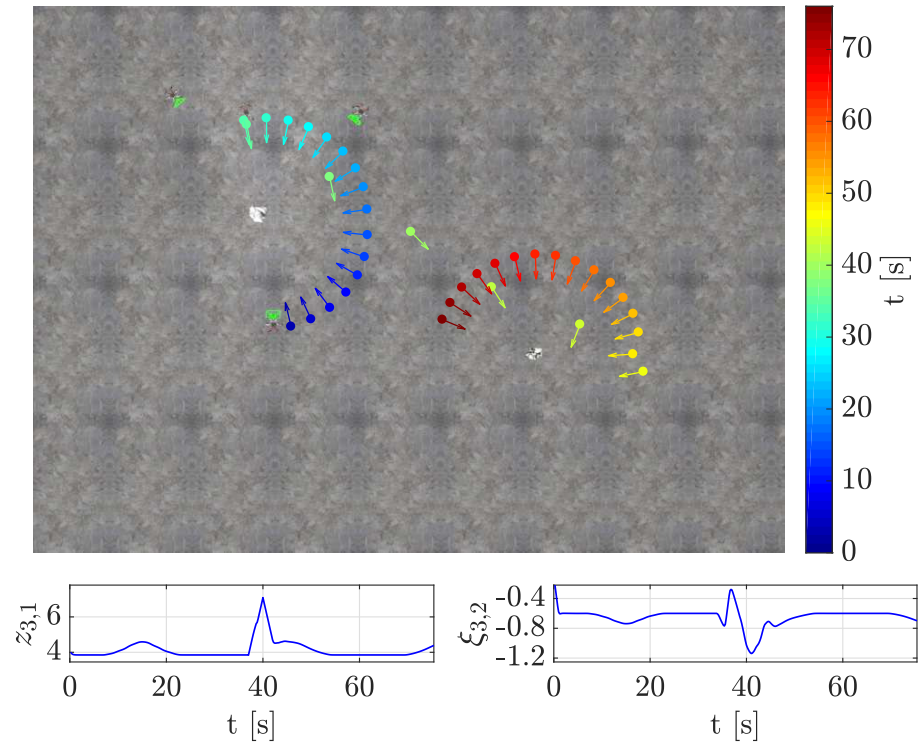

Fig. 19 The trajectory of the follower carrying the back light in the experiment with three lights (Subsection 7.1.2). The arrows denote the heading of light at particular times t.

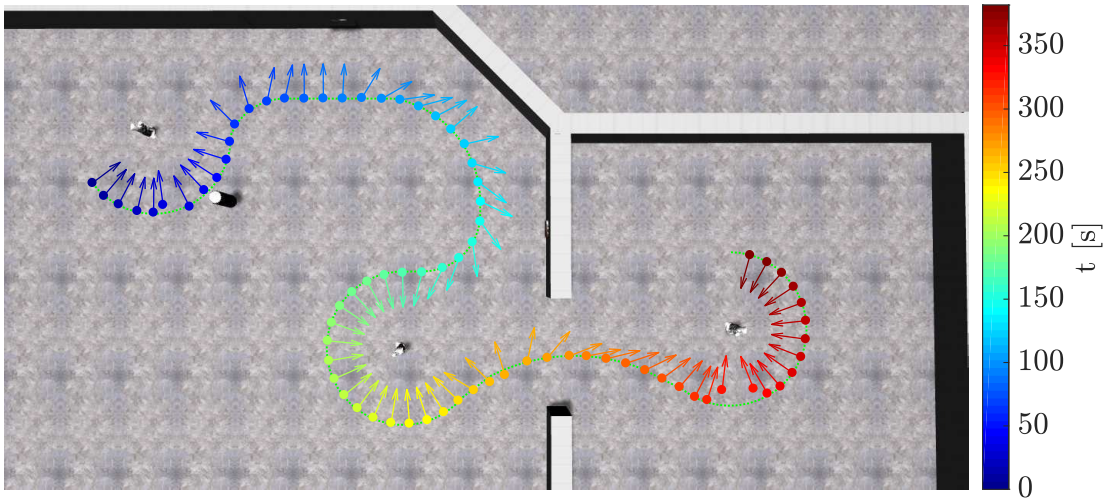

Fig. 20 The trajectory of the leader in the "2D experiment". The arrows denote the heading of the camera at particular times t, and the green dotted line shows the desired trajectory.

has gone through it. Therefore it reaches the desired position later than by using the 3D-approach.

Another disadvantage of the limitations on the change of altitude is shown in Fig. 22. It presents avoiding a faulty follower, which stays in the position that collides with the desired trajectories of other members of the formation. The leader avoids this follower without problems. However, when the second follower starts the avoidance manoeuvre, the path between the OoI and the faulty follower is already penalised and constrained by the constraint function $g_s(\cdot)$. Therefore, the follower has to choose the longer path beyond the faulty follower.

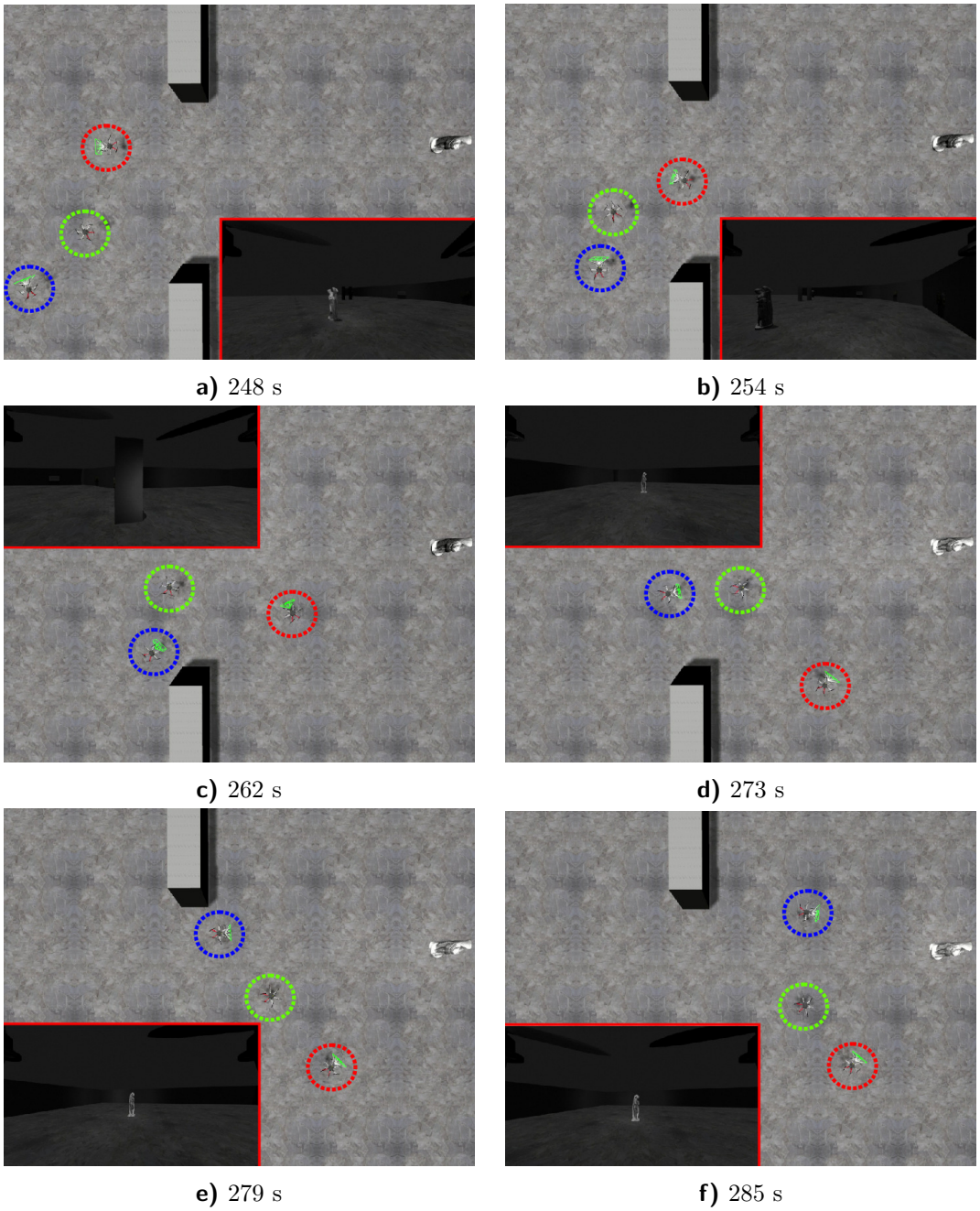

a) 248 s **b)** 254 s **c)** 262 s **d)** 273 s **e)** 279 s **f)** 285 s

Fig. 21 Snapshots of the formation during the transition to another OoI and concurrent avoiding to the obstacle in the experiment presented in Subsection 7.1.3. The dotted circles highlight the leader (green), the follower provided the key light (blue), and the follower provided the fill light (red). The corresponding camera shot is shown in the cut-out separated with the red line. (video: `https://youtu.be/jpJzaMv0G8s`)

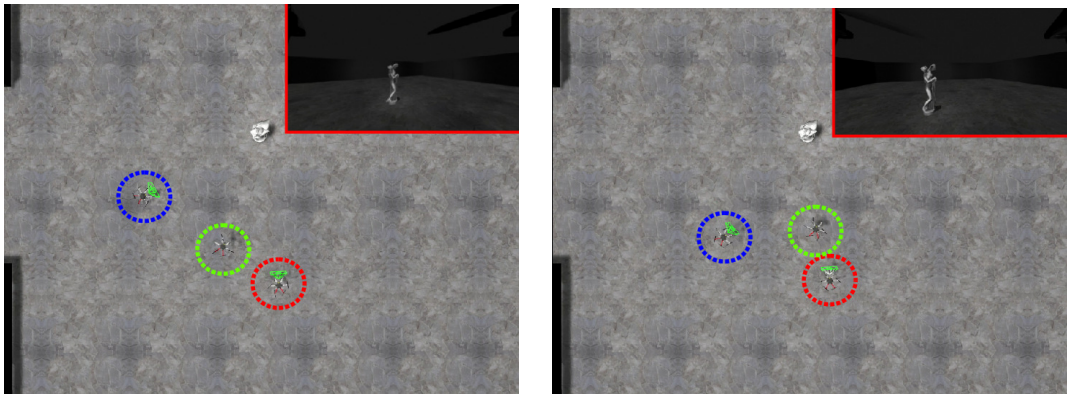

a) 307s **b)** 316 s

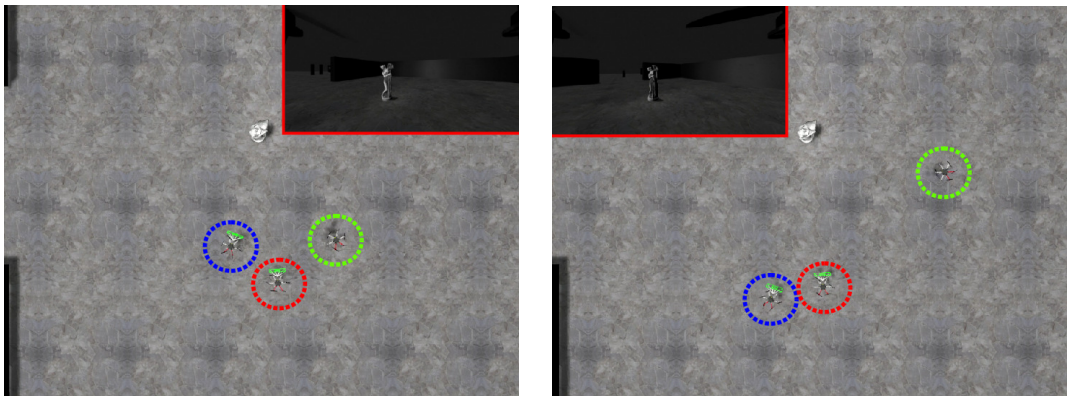

c) 325 s **d)** 340 s

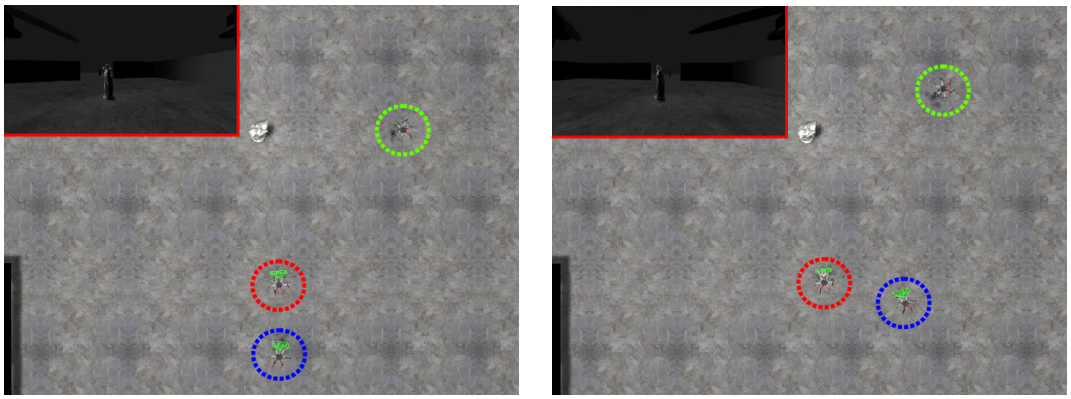

e) 347 s **f)** 354 s

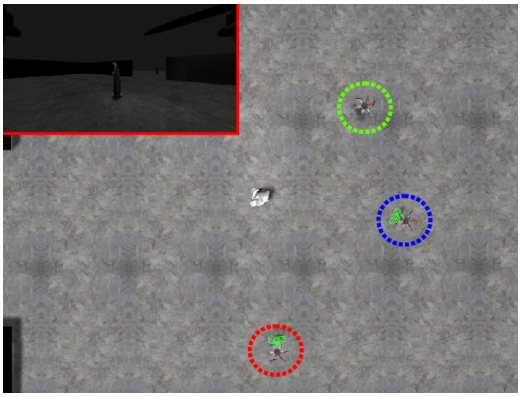

g) 364 s

Fig. 22 Snapshots of the formation during the avoiding the faulty follower. The dotted circles highlight the leader (green), the follower provided the key light (blue), and the follower provided the fill light (red). (video: `https://youtu.be/jpJzaMv0G8s`)

7.1.4 2D-modification - simple environment

In this environment (Fig. 23), we have verified the basic behaviour of the proposed system with 2D-modification. As the map and the desired distances from OoI are relatively small, they do not allow significant changes in altitude. Therefore, we set the desired altitude to all robots to the same value, and so all their trajectories lie in the same plane. This leads to the environment with many constraints.

We have realized three experiments in this environment. The first one is the experiment with trajectory with constant forward velocity. The only difference from the experiment presented in Subsection 7.1.3 is that the desired positions of the leader and followers are closer to each other and so the trajectories and positions of other members in the formation have a bigger influence on the behavior of particular robots. The constants (Tables 11, 12) used in this experiment and limitations on the control inputs (Table 10) are the same for all presented experiments in the simple environment. The trajectories of the robots in the formation (Fig. 41, 42, 43), graphs of the control inputs used for controlling the robots (Fig. 44), and graphs of the progress of the objective functions (Fig. 45) are presented in Appendix B. The experiment is captured in the video: `https://youtu.be/bDHShkQsNu4`, which is also located on the enclosed CD.

In the second one, we show the main advantage of using a trajectory instead of a path. It allows us to divide the assumed positions into two groups - the positions from which the camera should take the requested shots and the positions used only for the transition between the positions from the first group. Then it is possible to speed up during the transitions between OoIs and slow down or even stop in the desired positions for their scanning. It is useful especially for the attainment of desired lighting setup because the actual desired headings and positions of the followers are influenced by their desired headings and positions at the end of control horizon. By setting the desired trajectory of the leader in the way, that it scans the OoI from one position with constant heading for time $t_{scan} > NT_s$, we ensure that at a certain time each robot in the formation tries to participate on desired lighting setup and is not influenced by the next OoI. However, it does not mean that this setup will be accomplished. The position of robots can be still influenced by constraints and penalisations connected with all types of collisions including the presence in the shot. The trajectories of the leader and the followers (Fig. 36, 37, 38), graphs of the control inputs (Fig. 39) applied to the robots, and graphs of the progress of the objective functions (Fig. 40) are presented in Appendix B. The experiment is captured in the video `https://youtu.be/mZoN12Gb_0Q`, which is also located on the enclosed CD.

In the last experiment made in this environment, we added an obstacle into the map. The result shows the problem of the presented system with the obstacle avoidance. When the leader comes to the corridor between the last OoI and the obstacle, the actual heading $\theta_L(t)$, and bounds on the control inputs, does not allow it to go immediately through this corridor. Therefore the leader almost stopped and turned around to prepare for the successful avoidance manoeuvre. The found trajectory of the leader is shown in Fig. 23.

The follower stopped in front of the obstacle since most of its next N_F desired positions are within the constrained space and so it cannot go nearer to them. Therefore, it has no motivation to go through the corridor. When some of the desired positions are already outside the constrained space, the follower still stays in the same position. It stays there until the penalisation of the deviation from its desired position results in the higher penalty than the one given by the obstacle avoidance function and the functions penalising the fast changes in the sequence of control inputs. In this case, the

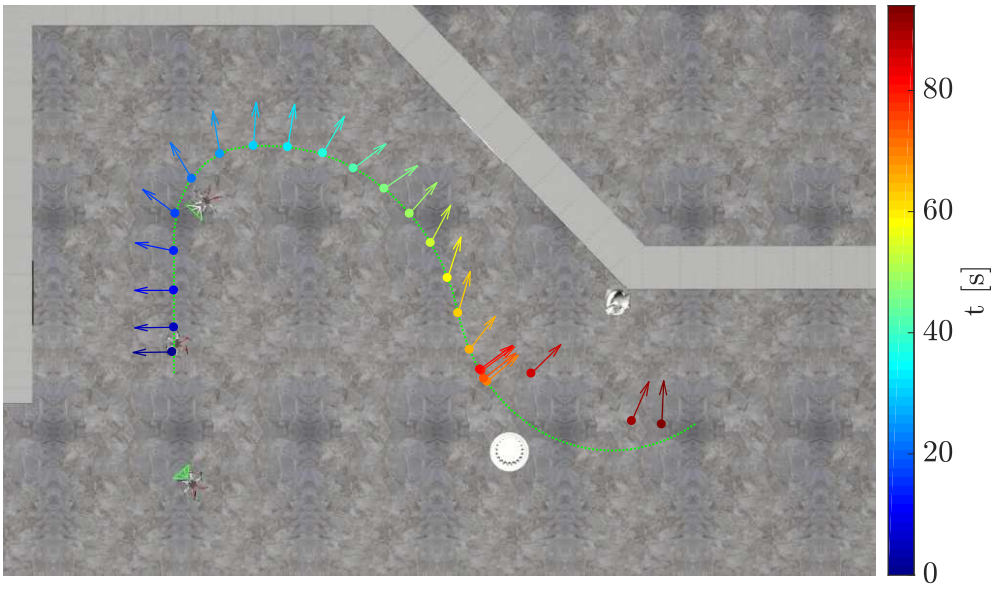

Fig. 23 The trajectory of the leader in the experiment in the simple environment with the obstacle. The arrows denote the heading of the camera at particular times t, and the green dotted line shows the desired trajectory.

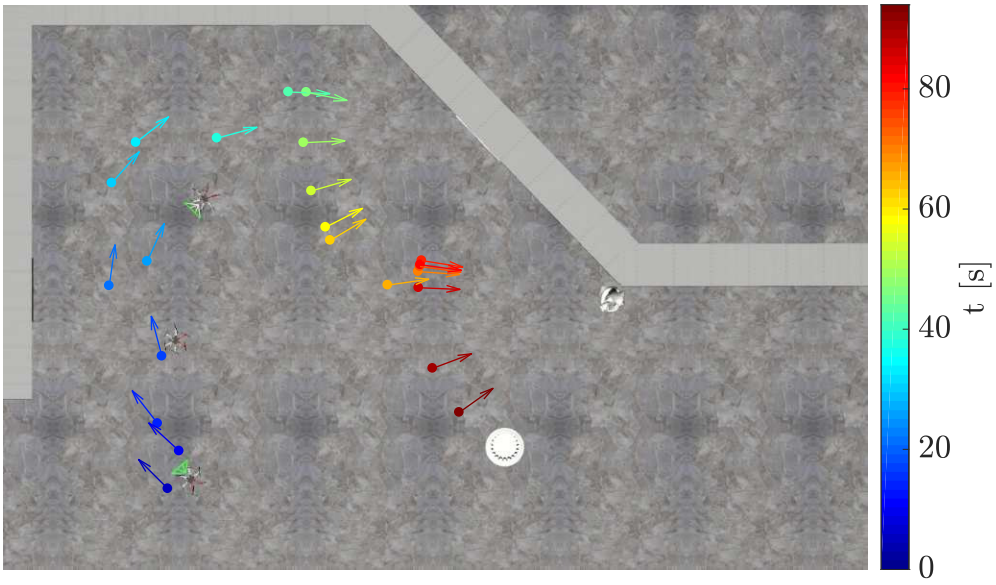

Fig. 24 The trajectory of the follower carrying the key light in the experiment in simple environment with the obstacle. The arrows denote the heading of the light at particular times t.

follower even has not move until the end of the mission. The trajectory of the follower carrying the key light is shown in Fig. 24. The trajectory of the follower provided the fill light (Fig 46), the graphs of the control inputs (Fig. 47) applied to the robots, and graphs of the progress of the objective functions (Fig. 48) are presented in Appendix B. The experiment is captured in the video `https://youtu.be/EHK-2rViZRU`, which is also located on the enclosed CD.

7.2 Real experiment

We have conducted the real experiment in the outdoor environment inspired by the map, which was used in the previous Subsection 7.1.4. The multi-rotor helicopters of Multi-robot Systems Group at Department of Cybernetics at FEE, CTU were used in this experiment. These robots are already equipped with the system for precise outdoor localization, controllers for trajectory tracking and the fixed camera on their frame. For our experiment, we used the camera only on the UAV, which represented the leader and we added the lights to the frames of followers (Fig. 25). Due to the unavailability of gimbals, we have realized the experiment only in the scenario for 2D-modification of the proposed method.

As we have already mentioned, the behaviour of the system should be verified in the simulation prior the mission. It enables the easier recognition of undesired behavior of the robot and consequently the faster reaction of a safety pilot, who is necesarry mainly in the initial algorithm testing. Since we have conducted the very first experiment with the presented system, we have used the precomputed trajectories from the simulation for controlling of robots movement.

The real experiment shows several issues, which were not noticeable from the simulations. Firstly, we suppose that the shadows caused by lighting through the leader will never appear in the FOV. Therefore we do not deal with it in the objective functions at all. Although the shadows have occurred several times within the FOV during this experiment, it has happened only during the transitions between the OoIs. Thus, it is not the problem for the expected application, and there is no reason for making the optimization tasks even more complicated.

The second issue, which we have noticed, is that the control of the camera heading is not so smooth as in the simulation. Nevertheless, the quality of measured data seems to be sufficient for assumed applications of the system. Moreover, the quality can be enhanced by utilization of the gimbal, which is able to stabilize the camera and ensure

Fig. 25 The multi-rotor helicopter equipped with the light, which was deployed in the real experiment.

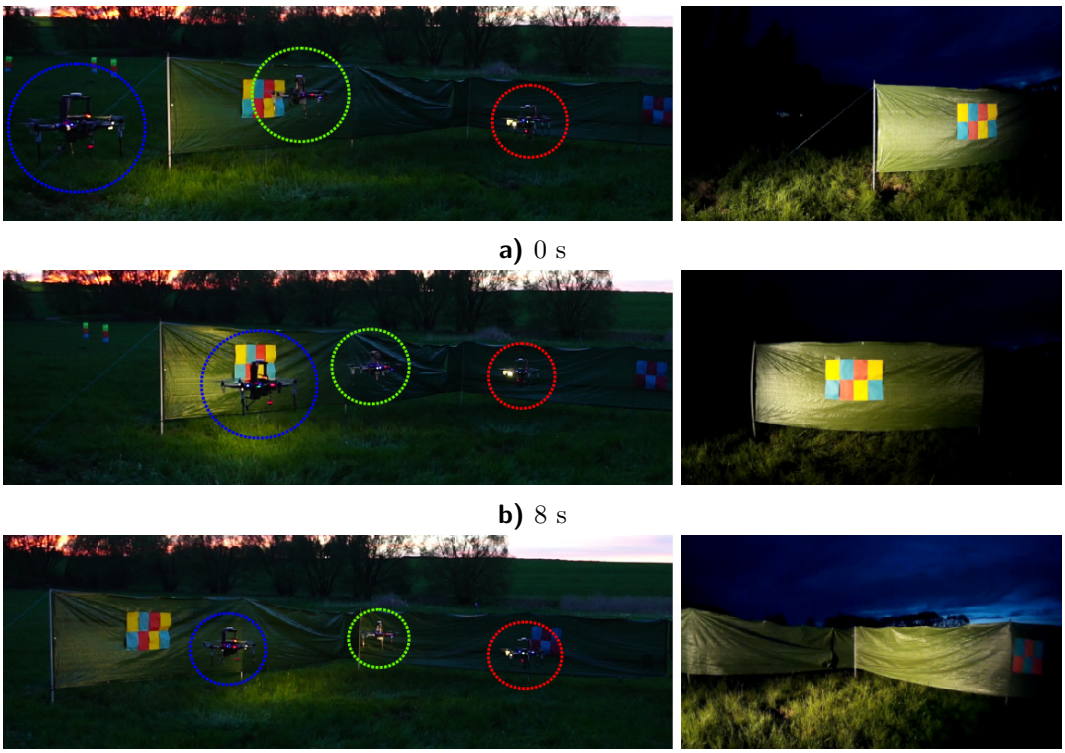

a) 0 s

b) 8 s

c) 17 s

Fig. 26 The photos of the formation at particular times of the real experiment (left side) and the photos cut out from the video taken by the camera mounted on the frame of the leader at corresponding times (right side). The dotted circles highlight the leader (green), the follower provided the key light (blue), and the follower provided the fill light (red). (video: `https://youtu.be/CuXX3hlA7Hk`)

its smoother rotations.

The photos of the formation during the experiment together with the photos cut out from the video taken by the camera mounted on the frame of the leader are shown in Fig. 26, 27. The green canvases are the obstacles, which are known to the robots, the colourful areas denote the flat OoIs, and the multi-coloured column stands for the three-dimensional object of interest. Since different light conditions are suitable for the filming of the formation and the visibility of followers lights, we conducted the experiment also more times in different light conditions. Therefore the background is darker in the images from the camera than in the images of the formation. The experiment is captured in the video `https://youtu.be/CuXX3hlA7Hk`, which is also located on the enclosed CD.

Let us present two most important findings based on the real experiment. Firstly, the limitations on the ascent, forward and angular velocities of the robots applied in the simulations are feasible also for the real robots. And secondly, the robots are capable of working also in such a small distances as in the simulation experiments. It is the crucial assumption for deployment of the system in an indoor environment which is often confined, and it also enables the use of lightweight light sources with lower light intensity. Nevertheless, we expect the application of smaller UAVs with propeller guards, which decrease the chance of the damage of the robots and the surrounding environment in the case of a collision.

a) 24 s

b) 37 s

c) 50 s

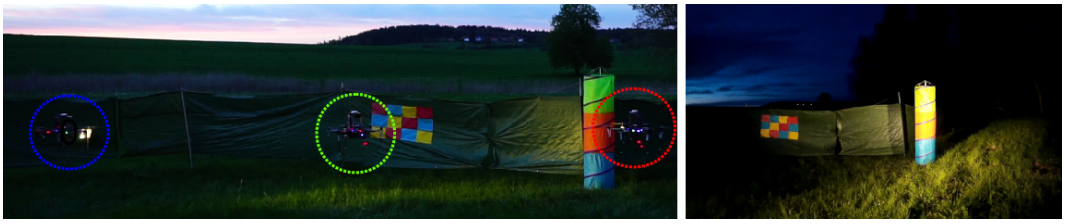

d) 65 s

e) 80 s

f) 100 s

Fig. 27 The photos of the formation at particular times of the real experiment (left side) and the photos cut out from the video taken by the camera mounted on the frame of the leader at corresponding times (right side). The dotted circles highlight the leader (green), the follower provided the key light (blue), and the follower provided the fill light (red). (video: `https://youtu.be/CuXX3hlA7Hk`)

8 Conclusion

The system for control and stabilization of a formation of UAVs used for filming in dark conditions is presented in this work. The method is based on the leader-follower approach and model predictive control on a receding horizon. The definition of the proposed objective functions and constraints used within the MPC scheme are presented in Section 5. They take into account collisions with obstacles, collisions with other robots in the formation, limitations on control inputs and presence of a follower in the FOV of the camera.

We have verified the system in numerous experiments in simulations. Based on these experiments, we can conclude that the proposed methods are capable of working with a different number of followers carrying the light sources and accepting various limitations on control inputs. Apart from the presented 3D approach, we have also tested some modifications of this system, which are advantageous for specific applications. We focus especially on the 2D-modification, which decreases the demands on the hardware of the robots. Apart of the lower computational demands in comparison to the 3D approach, the robots also do not need to be equipped with gimbals.

On the ground of simulation results, we have successfully realized the real experiment in the outdoor modeled scenario. It shows that the limitations on the motion of the robot used in the simulation were sufficient and the UAVs are competent to fly as close to each other as in the simulation experiments. Nevertheless, in the case of indoor experiments, it seems that the use of smaller robots can be more appropriate and safer.

The proposed method is prepared to be integrated into the system of Multi-Robot-Systems group at Department of Cybernetics at FEE, CTU. It can be employed for scanning of cultural heritage sites using the three point lighting scheme or strong side lighting approach. The essential condition for usage of this system in indoor environments is the integration of the system for precise indoor localization, that can be based on the optical flow and relative localization. For the strong side lighting, the multi-rotors has to be also equipped with the reliable collision avoidance system, which allows them to fly very close to the walls. In general, the number of possible applications can be extended with the increasing guarantee of safety.

Finally, let us emphasize that the presented work was already positivelly appreciated by robotics community, especially by reviewers of two accepted conference papers with included results of this thesis [36], [37].

References

[1] Multi-robot Systems group. *CESNET*. 2017. URL: `http://mrs.felk.cvut.cz/projects/cesnet` (visited on 04/05/2017).

[2] W. Sheng et al. "Visual Point-based Analysis of Laser-scanned Historical Structures". In: *IEEE International Conference on Culture and Computing*. 2015, pp. 47–53.

[3] N.-J. Shih et al. "3D scan for the digital preservation of a historical temple in Taiwan". In: *Advances in Engineering Software* 38.7 (2007), pp. 501–512.

[4] R. Zlot et al. "Efficiently capturing large, complex cultural heritage sites with a handheld mobile 3D laser mapping system". In: *Journal of Cultural Heritage* 15.6 (2014), pp. 670–678.

[5] P. S. Blear and P. K. Allen. "Data Acquisition and View Planning for 3-D Modeling Tasks". In: *IEEE International Conference on Intelligent Robots and Systems*. 2007.

[6] M. Hess et al. "Fusion of Multimodal Three-dimensional Data for Comprehensive Digital Documentation of Cultural Heritage Sites". In: *Digital Heritage*. 2015.

[7] N. Hallermann et al. "Vision-based monitoring of heritage monuments: Unmanned Aerial Systems(UAS) for detailed inspection and high-accuracy survey of structures". In: *IEEE Transactions on Cybernetics* 45.5 (2015), pp. 869–879.

[8] L. Wei et al. "3D Modeling Based on Multiple Unmanned Aerial Vehicles with the Optimal Paths". In: *IEEE International Symposium on Intelligent Signal Processing and Communication Systems*. 2016, pp. 1–6.

[9] C. Teuliere et al. "3-D Model-Based Tracking for UAV Indoor Localization". In: *IEEE Transactions on Cybernetics* 45.5 (2015), pp. 869–879.

[10] S. Minaeian et al. "Vision-Based Target Detection and Localization via a Team of Cooperative UAV and UGVs". In: *IEEE Transactions on Systems, Man, and Cybernetics: Systems* 46.7 (2016), pp. 1005–1016.

[11] J. Faigl et al. "Low-Cost Embedded System for Relative Localization in Robotic Swarms". In: *IEEE International Conference on Robotics and Automation (ICRA)*. 2013.

[12] T. Krajník et al. "A Practical Multirobot Localization System". In: *Journal of Intelligent and Robotic Systems* 76.3-4 (2014), pp. 539–562.

[13] M. Saska. "MAV-swarms: unmanned aerial vehicles stabilized along a given path using onboard relative localization". In: *International Conference on Unmanned Aircraft Systems (ICUAS)*. 2015.

[14] M. Saska et al. "Swarms of Micro Aerial Vehicles Stabilized Under a Visual Relative Localization". In: *IEEE International Conference on Robotics and Automation (ICRA)*. 2014.

[15] M. Saska et al. “Swarm Distribution and Deployment for Cooperative Surveillance by Micro-Aerial Vehicles”. In: *Journal of Intelligent and Robotic Systems.* 84.1 (2016), pp. 469–492.

[16] M. Saska et al. “Autonomous Deployment of Swarms of Micro-Aerial Vehicles in Cooperative Surveillance”. In: *International Conference on Unmanned Aircraft Systems (ICUAS).* 2014.

[17] M. A. Kamel and Y. Zhang. “Decentralized leader-follower formation control with obstacle avoidance of multiple unicycle mobile robots”. In: *2015 IEEE 28th Canadian Conference on Electrical and Computer Engineering (CCECE).* 2015, pp. 406–411.

[18] Z. Weihua and T. H. Go. “Robust cooperative Leader-follower formation flight control”. In: *2010 11th International Conference on Control Automation Robotics Vision.* 2010, pp. 275–280.

[19] A. Bemporad and C. Rocchi. “Decentralized linear time-varying model predictive control of a formation of unmanned aerial vehicles”. In: *2011 50th IEEE Conference on Decision and Control and European Control Conference.* 2011, pp. 7488–7493.

[20] M. Saska et al. “Coordination and Navigation of Heterogeneous MAV-UGV Formations Localized by a ’hawk-eye’-like Approach Under a Model Predictive Control Scheme”. In: *International Journal of Robotics Research* 33.10 (2014), pp. 1393–1412.

[21] M. Saska et al. “Fault-Tolerant Formation Driving Mechanism Designed for Heterogeneous MAVs-UGVs Groups”. In: *Journal of Intelligent and Robotic Systems* 73.1-4 (2014), pp. 603–622.

[22] V. Spurný et al. “Complex manoeuvres of heterogeneous MAV-UGV formations using a model predictive control”. In: *21st International Conference on Methods and Models in Automation and Robotics (MMAR).* 2016.

[23] M. Saska et al. “Motion Planning and Control of Formations of Micro Aerial Vehicles”. In: *19th World Congress of the International Federation of Automatic Control (IFAC).* 2014.

[24] M. Saska et al. “Navigation, Localization and Stabilization of Formations of Unmanned Aerial and Ground Vehicles”. In: *International Conference on Unmanned Aircraft Systems (ICUAS).* 2013.

[25] M. Saska et al. “Coordination and Navigation of Heterogeneous UAVs-UGVs Teams Localized by a Hawk-Eye Approach”. In: *IEEE/RSJ International Conference on Intelligent Robots and Systems (IROS).* 2012.

[26] M. Saska et al. “Formations of Unmanned Micro Aerial Vehicles Led by Migrating Virtual Leader”. In: *14th International Conference on Control, Automation, Robotics and Vision (ICARCV).* 2016.

[27] E. F. Camacho and C. Bordons. *Model Predictive Control. Advanced Textbooks in Control and Signal Processing.* 2nd ed. London: Springer, 2007. Chap. Introduction to Model Predictive Control, pp. 1–12. ISBN: 978-1-85233-694-3.

[28] M. Saska et al. “Control and Navigation of Formations of Car-Like Robots on a Receding Horizon”. In: *IEEE Multi-conference on Systems and Control.* 2009.

[29] Y. Zhang and K. L. Ma. “Lighting Design for Globally Illuminated Volume Rendering”. In: *IEEE Transactions on Visualization and Computer Graphics* 19.12 (2013), pp. 2946–2955.

[30] B. Jeremy. *Digital Lighting and Rendering*. 1st ed. Indianapolis: New Riders, 2000. Chap. 3 - Three Points Lighting, pp. 34–61. ISBN: 1-56205-954-8.

[31] I. Hymann. *Three point lighting: Learn how to use the key, fill, and back lights*. 2011. URL: `http://www.izzyvideo.com/three-point-lighting/` (visited on 03/03/2017).

[32] D. Shreiner et al. *OpenGL Programming Guide. The Official Guide to Learning OpenGL*. 8th ed. Michigan: Pearson Education, 2013. Chap. 7 - Light and Shadow, pp. 368–409. ISBN: 978-0321773036.

[33] D. M. Stipanović et al. “Cooperative avoidance control for multi-agent systems”. In: *Journal of Dynamic Systems, Measurement, and Control* 129.5 (2007), pp. 699–707.

[34] M. Saska et al. “Predictive control and stabilization of nonholonomic formations with integrated spline-path planning”. In: *Robotics and Autonomous Systems* 75.Part B (2016), pp. 379–397.

[35] C. Lawrence et al. *User’s Guide for CFSQP Version 2.5*. 1997.

[36] V. Kratky et al. “Documentation of large historical buildings by UAV formations - scene perception-driven motion planning and predictive control”. In: *IEEE Multi-robot Perception-Driven Control and Planning (ICRA)*. expected 2017.

[37] M. Saska et al. “Documentation of Dark Areas of Large Historical Buildings by a Formation of Unmanned Aerial Vehicles using Model Predictive Control”. In: *IEEE ETFA*. expected 2017.

Appendix A

CD content

The content of the CD is described in Table 4.

Directory name	Description
thesis	thesis in pdf format
sources	source codes of program
videos	videos from experiments

Tab. 4 CD content

Appendix B

Additional experimental results

Experiment with three lights

$\alpha\,[-]$	$\beta_1\,[-]$	$\beta_2\,[-]$	$\beta_3\,[-]$	$\gamma\,[-]$	$\delta\,[-]$	$N\,[-]$	$r_{s,o}[m]$	$r_{s,r,L}[m]$	$AoV_h[rad]$
1	0.1	0.1	0.1	0.2	0.5	13	2.5	2.5	1.85
$\eta\,[-]$	$\zeta_1\,[-]$	$\zeta_2\,[-]$	$\kappa_1\,[-]$	$\kappa_2\,[-]$	$T_s[s]$	$n\,[-]$	$r_{a,o}[m]$	$r_{a,r,L}[m]$	$AoV_v[rad]$
0.5	1	1	0.01	0.01	0.4	1	1.5	1.5	1.57

Tab. 5 The constants used in the optimization task of the leader in the experiment presented in Subsection 7.1.2.

$\mu\,[-]$	$\lambda_1\,[-]$	$\lambda_2\,[-]$	$\lambda_3\,[-]$	$\nu\,[-]$	$\tau\,[-]$	$d_{cs}\,[m]$	$N_F\,[-]$	$r_{s,o}[m]$	$r_{s,r,F}[m]$	$d_1[m]$	$\sigma_1\,[-]$	$\sigma_3\,[-]$
1	0.2	0.2	0.4	1	2	2	12	2.5	3.5	4.47	1	0.7
$\iota\,[-]$	$\vartheta\,[-]$	$\epsilon_1\,[-]$	$\epsilon_2\,[-]$	$\varsigma_1\,[-]$	$\varsigma_2\,[-]$	$T_s[s]$	$n\,[-]$	$r_{a,o}[m]$	$r_{a,r,Fd}[m]$	$d_2[m]$	$\sigma_2\,[-]$	$d_3[m]$
2	1	1	1	0.05	0.05	0.4	1	1.5	2.5	5.47	0.7	3.87

Tab. 6 The constants used in the optimization task of the followers in the experiment presented in Subsection 7.1.2.

j	L - leader	1 - key light	2 - fill light	3 - back light
$v_{j,min}[\mathrm{m\,s^{-1}}]$	0.075	−0.6	−0.6	−0.9
$v_{j,max}[\mathrm{m\,s^{-1}}]$	0.5	0.6	0.6	0.9
$K_{j,min}[m^{-1}]$	−2	−2	−2	−2
$K_{j,max}[m^{-1}]$	2	2	2	2
$w_{j,min}[\mathrm{m\,s^{-1}}]$	−0.5	−0.6	−0.6	−0.6
$w_{j,max}[\mathrm{m\,s^{-1}}]$	0.5	0.6	0.6	0.6
$\omega_{j,min}[\mathrm{rad\,s^{-1}}]$	−0.1	−0.25	−0.25	−0.25
$\omega_{j,max}[\mathrm{rad\,s^{-1}}]$	0.1	0.25	0.25	0.25
$\varepsilon_{j,min}[\mathrm{rad\,s^{-1}}]$	−0.2	−0.25	−0.25	−0.25
$\varepsilon_{j,max}[\mathrm{rad\,s^{-1}}]$	0.2	0.25	0.25	0.25

Tab. 7 The limitations on control inputs used in the experiment presented in Subsection 7.1.2.

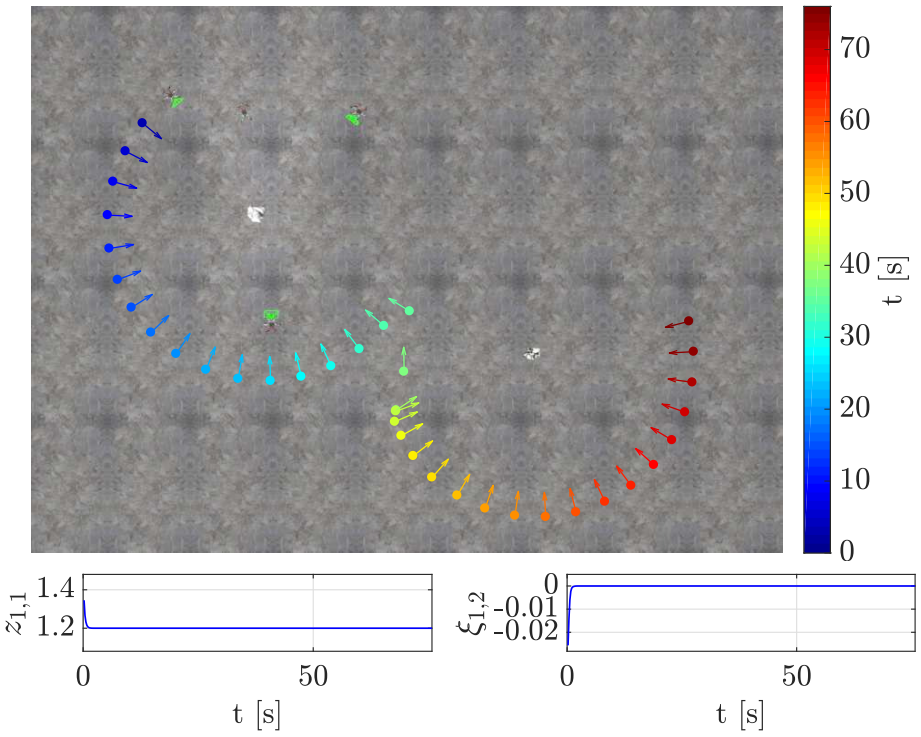

Fig. 28 The trajectory of the follower carrying the key light in the experiment with three lights (Subsection 7.1.2). The arrows denote the heading of light at particular times t.

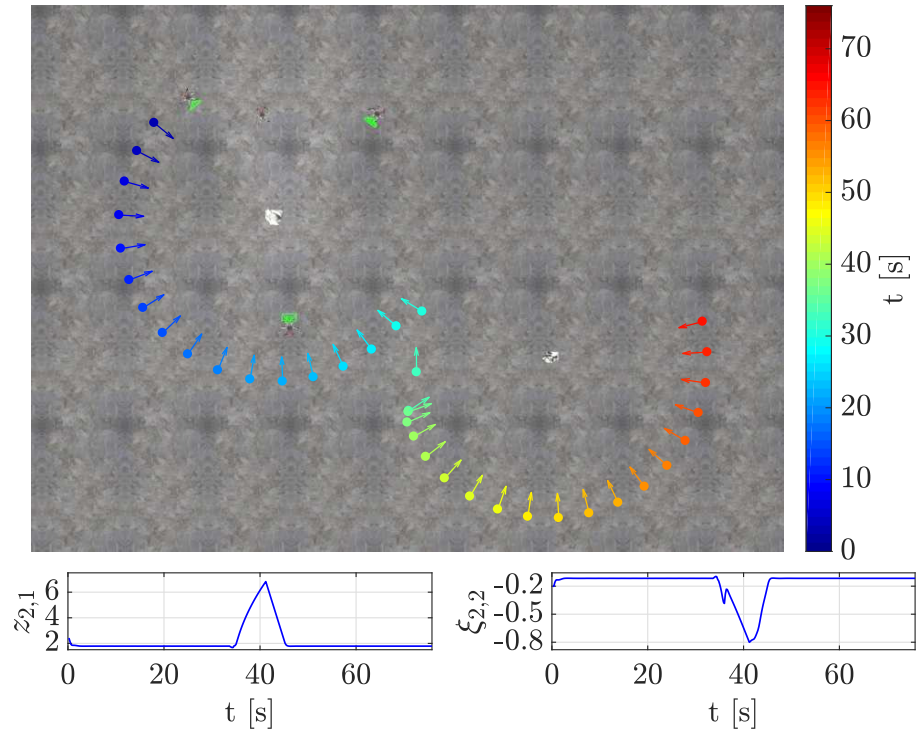

Fig. 29 The trajectory of the follower carrying the fill light in the experiment with three lights (Subsection 7.1.2). The arrows denote the heading of light at particular times t.

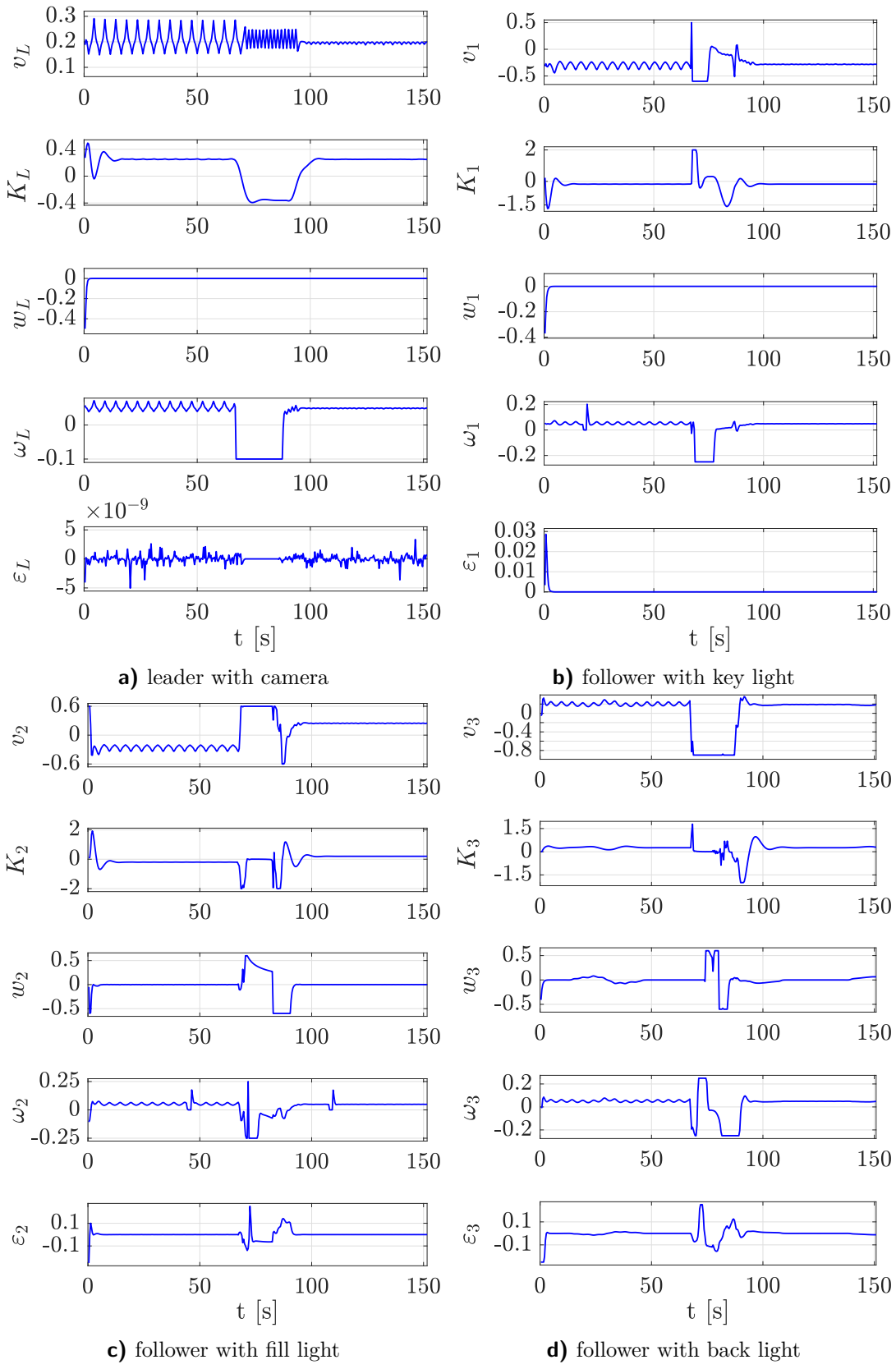

Fig. 30 Control inputs used for controlling of the robots in the experiment with three lights presented in Subsection 7.1.2.

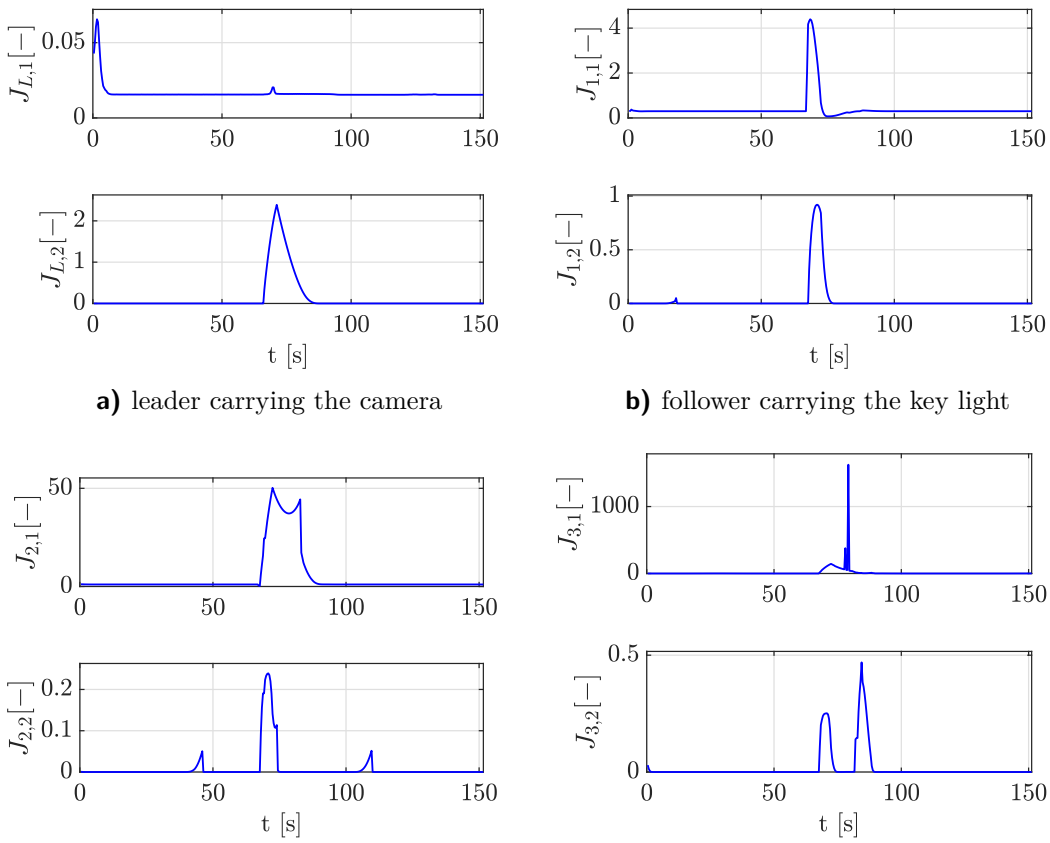

a) leader carrying the camera

b) follower carrying the key light

c) follower carrying the fill light

d) follower carrying the back light

Fig. 31 The progress of the values of the objective functions used for trajectory tracking and heading control of particular robots in the experiment with three lights presented in Subsection 7.1.2.

2D-modification

$\alpha\,[-]$	$\beta_1\,[-]$	$\beta_2\,[-]$	$\beta_3\,[-]$	$\gamma\,[-]$	$\delta\,[-]$	$N\,[-]$	$r_{s,o}[m]$	$r_{s,r,L}[m]$	$AoV_h[rad]$
2	0.1	0.1	-	0.1	1	12	2.5	2.5	1.9
$\eta\,[-]$	$\zeta_1\,[-]$	$\zeta_2\,[-]$	$\kappa_1\,[-]$	$\kappa_2\,[-]$	$T_s[s]$	$n\,[-]$	$r_{a,o}[m]$	$r_{a,r,L}[m]$	$AoV_v[rad]$
0.5	1	-	0.01	-	0.2	1	1.5	1.5	1.57

Tab. 8 The constants used in the optimization task of the leader in the experiment presented in Subsection 7.1.3.

$\mu\,[-]$	$\lambda_1\,[-]$	$\lambda_2\,[-]$	$\lambda_3\,[-]$	$\nu\,[-]$	$\tau\,[-]$	$d_{cs}\,[m]$	$N_F\,[-]$	$r_{s,o}[m]$	$r_{s,r,F}[m]$	$d_1[m]$	$\sigma_1\,[-]$
4.5	0.1	0.1	-	0.1	0.1	1.5	11	2.5	2.5	4.47	1
$\iota\,[-]$	$\vartheta\,[-]$	$\epsilon_1\,[-]$	$\epsilon_2\,[-]$	$\varsigma_1\,[-]$	$\varsigma_2\,[-]$	$T_s[s]$	$n\,[-]$	$r_{a,o}[m]$	$r_{a,r,Fd}[m]$	$d_2[m]$	$\sigma_2\,[-]$
0.4	0.1	1	-	0.05	-	0.2	2	1.5	1.75	5.0	0.7

Tab. 9 The constants used in the optimization task of the followers in the experiment presented in Subsection 7.1.3.

j	L - leader	1 - key light	2 - fill light
$v_{j,min}[\mathrm{m\,s^{-1}}]$	0.03	−0.48	−0.48
$v_{j,max}[\mathrm{m\,s^{-1}}]$	0.50	0.48	0.48
$K_{j,min}[m^{-1}]$	−2.00	−2.00	−2.00
$K_{j,max}[m^{-1}]$	2.00	2.00	2.00
$\omega_{j,min}[\mathrm{rad\,s^{-1}}]$	−0.10	−0.10	−0.10
$\omega_{j,max}[\mathrm{rad\,s^{-1}}]$	0.10	0.10	0.10

Tab. 10 The limitations on the control inputs used for control of the robots in the experiments presented in Subsection 7.1.3 and 7.1.4 .

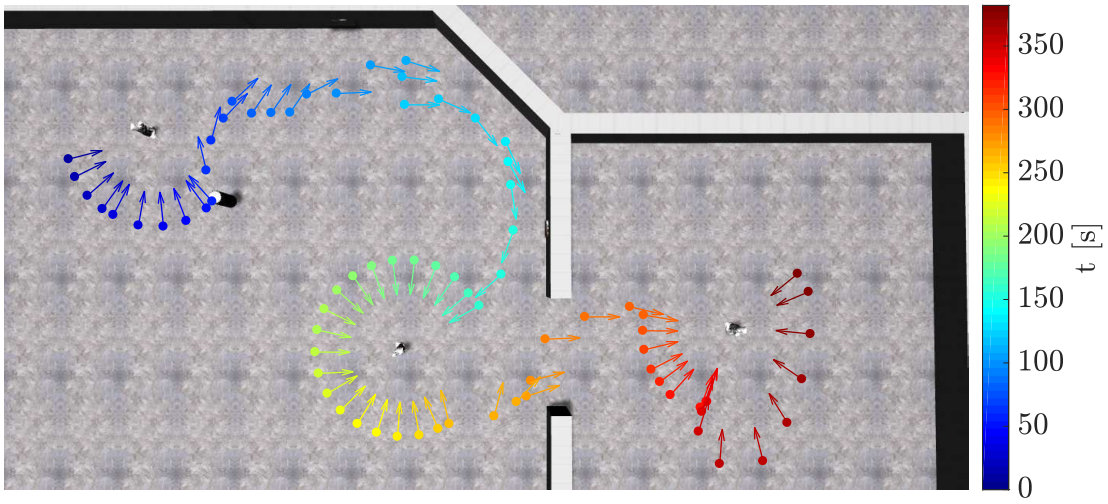

Fig. 32 The trajectory of the follower carrying the key light in the 2D experiment (Subsection 7.1.3). The arrows denote the heading of the light at particular times t.

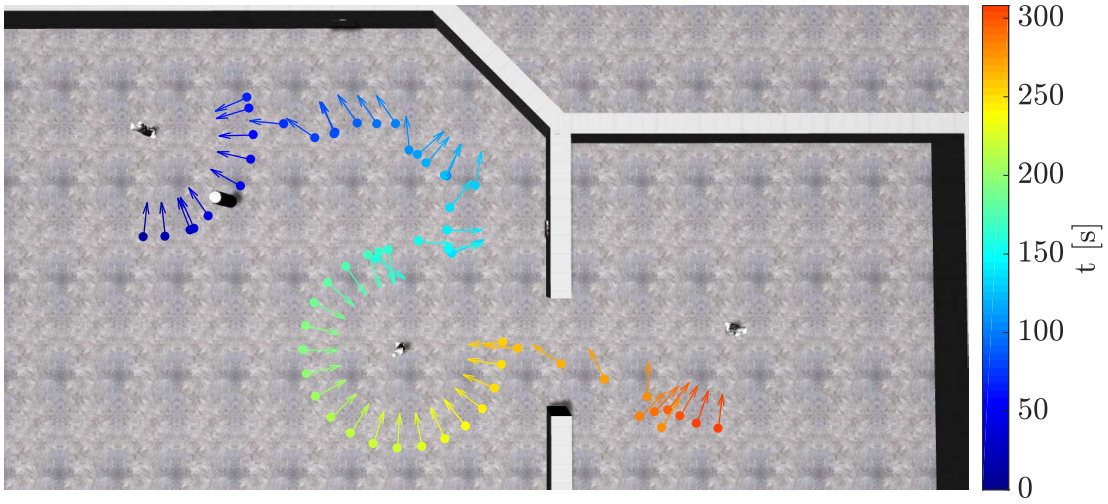

Fig. 33 The trajectory of the follower carrying the fill light in the 2D experiment (Subsection 7.1.3). The arrows denote the heading of the light at particular times t.

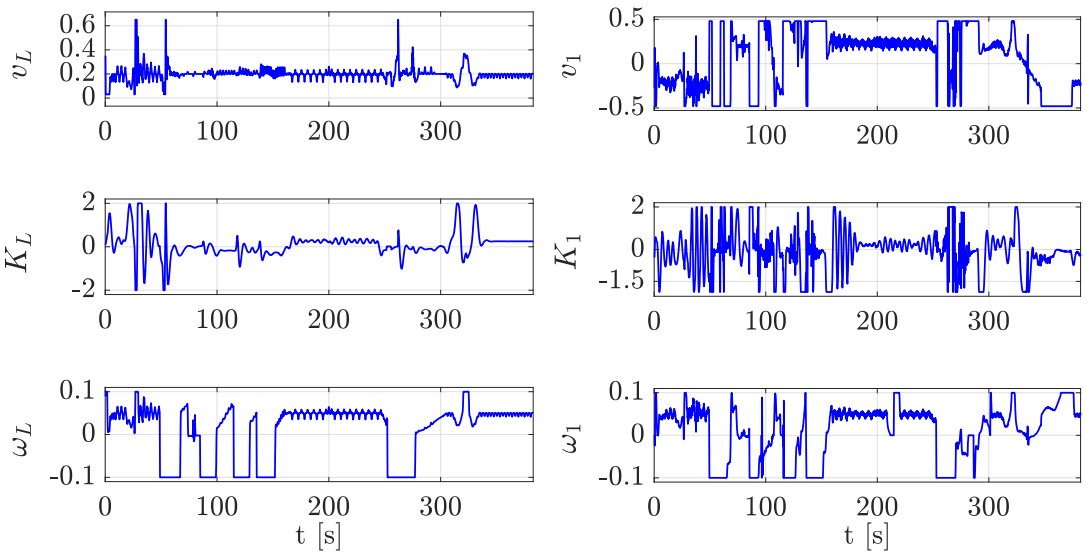

a) leader with camera **b)** follower with key light

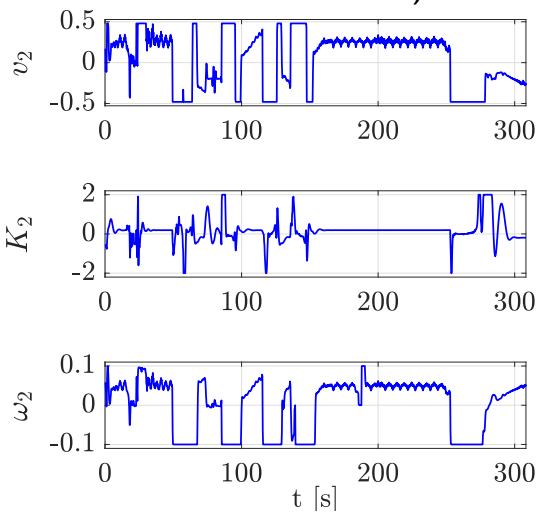

c) follower with fill light

Fig. 34 Control inputs used for controlling of the robots in the experiment presented in Subsection 7.1.3.

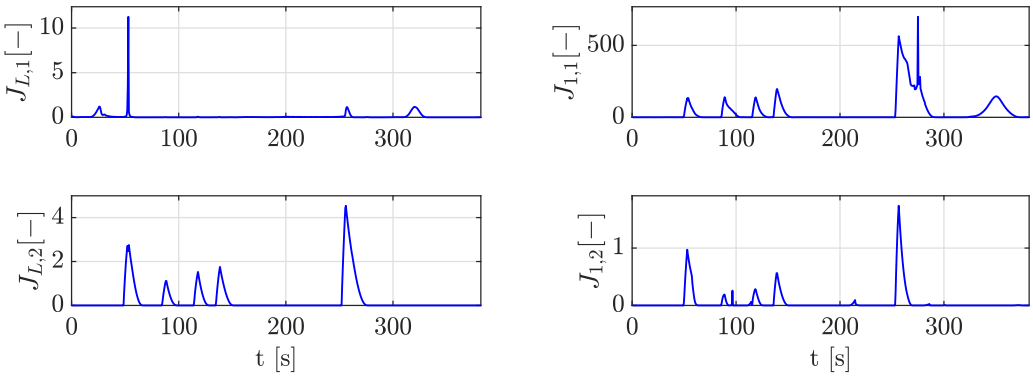

a) leader carrying the camera

b) follower carrying the key light

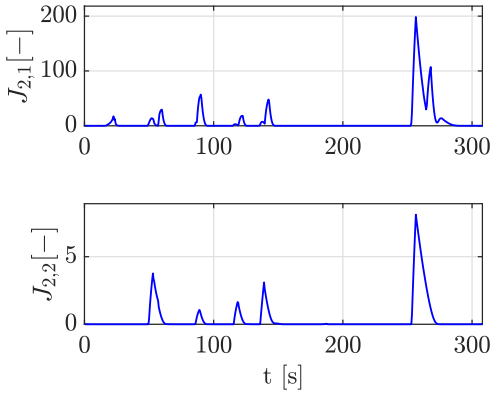

c) follower carrying the fill light

Fig. 35 The progress of the values of the objective functions used for trajectory tracking and heading control of particular robots in the experiment presented in Subsection 7.1.3.

Simple environment

α [−]	β_1 [−]	β_2 [−]	β_3 [−]	γ [−]	δ [−]	N [−]	$r_{s,o}[m]$	$r_{s,r,L}[m]$	$AoV_h[rad]$
2	0.1	0.1	-	0.1	1	12	2.5	2.5	1.9
η [−]	ζ_1 [−]	ζ_2 [−]	κ_1 [−]	κ_2 [−]	$T_s[s]$	n [−]	$r_{a,o}[m]$	$r_{a,r,L}[m]$	$AoV_v[rad]$
0.5	1	-	0.01	-	0.2	1.2	1.5	1.5	1.57

Tab. 11 The constants used in the optimization task of the leader in the experiment presented in Subsection 7.1.4.

μ [−]	λ_1 [−]	λ_2 [−]	λ_3 [−]	ν [−]	τ [−]	d_{cs} [m]	N_F [−]	$r_{s,o}[m]$	$r_{s,r,F}[m]$	$d_1[m]$	σ_1 [−]
2	0.1	0.1	-	0.3	0.3	2	11	2.5	2.5	4.47	1
ι [−]	ϑ [−]	ϵ_1 [−]	ϵ_2 [−]	ς_1 [−]	ς_2 [−]	$T_s[s]$	n [−]	$r_{a,o}[m]$	$r_{a,r,Fd}[m]$	$d_2[m]$	σ_2 [−]
0.6	0.3	1	-	0.05	-	0.2	1	1.5	1.75	5.0	0.7

Tab. 12 The constants used in the optimization task of the followers in the experiment presented in Subsection 7.1.4.

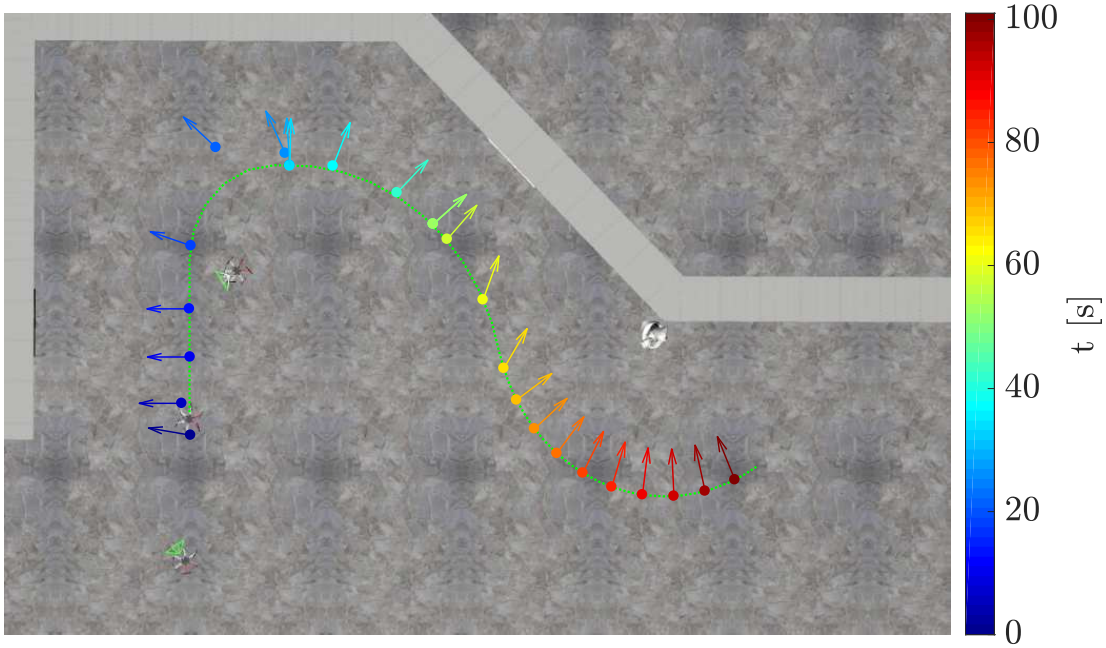

Fig. 36 The trajectory of the leader in the experiment with variable segmented trajectory presented in Subsection 7.1.4. The arrows denote the camera heading at particular times t, and the green dotted line shows the desired trajectory.

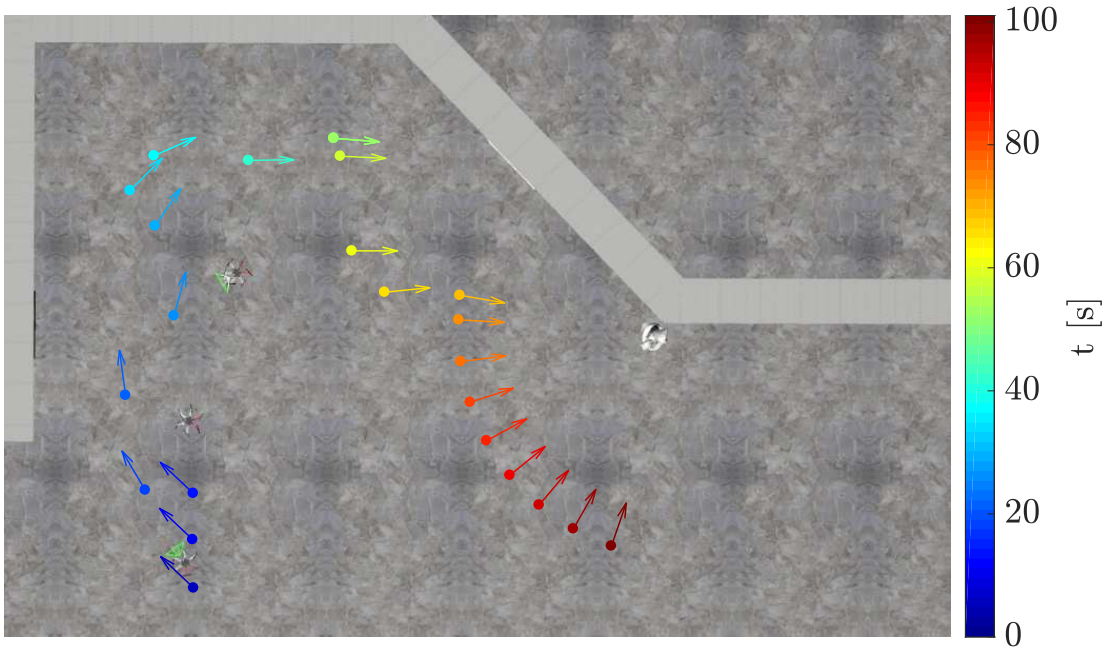

Fig. 37 The trajectory of the follower carrying the key light in the experiment with variable segmented trajectory presented in Subsection 7.1.4. The arrows denote the heading of the light at particular times t, and the green dotted line shows the desired trajectory.

Fig. 38 The trajectory of the follower carrying the fill light in the experiment with variable segmented trajectory presented in Subsection 7.1.4. The arrows denote the heading of the light at particular times t, and the green dotted line shows the desired trajectory.

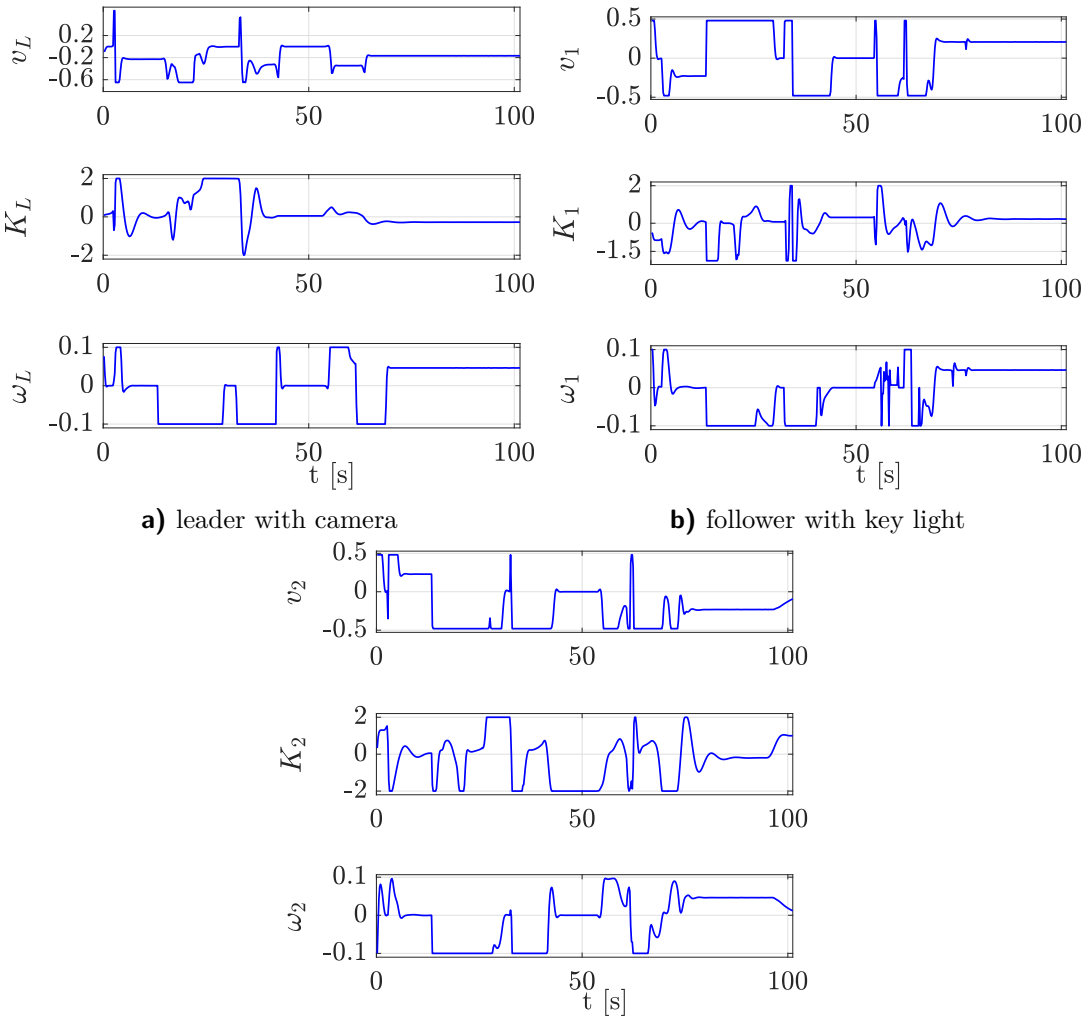

a) leader with camera

b) follower with key light

c) follower with fill light

Fig. 39 Control inputs used for controlling of robots in the experiment presented in Subsection 7.1.4 - variable segmented trajectory.

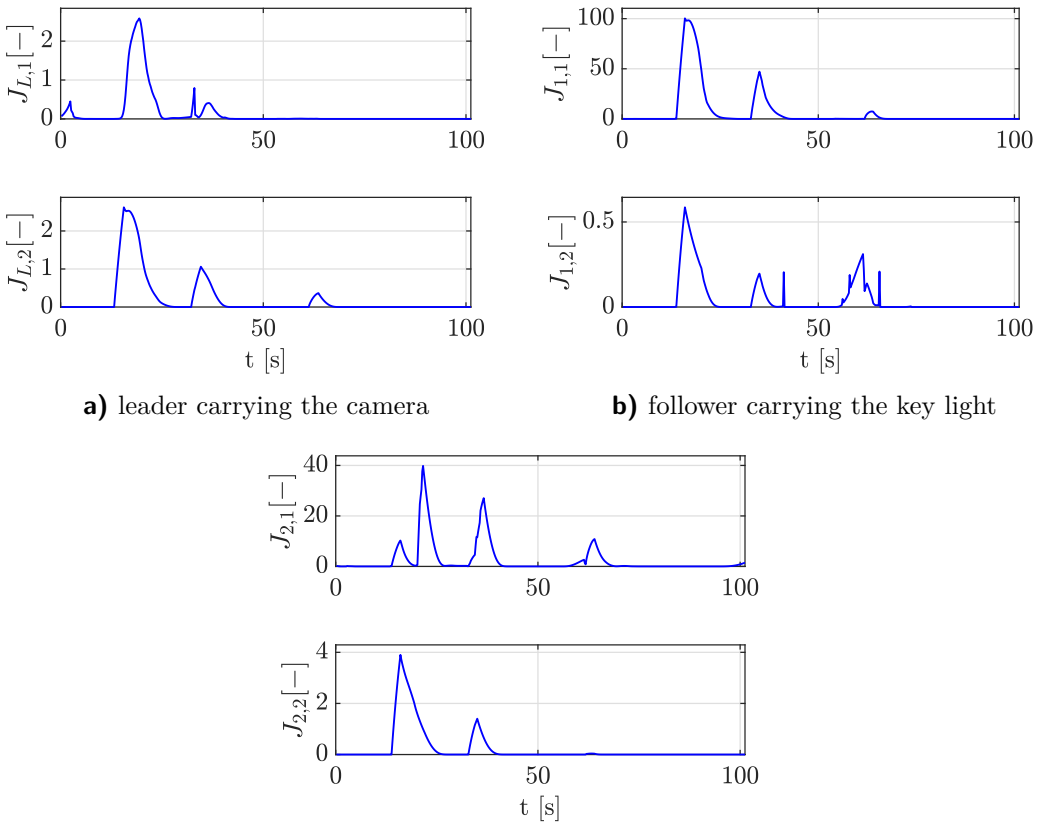

a) leader carrying the camera

b) follower carrying the key light

c) follower carrying the fill light

Fig. 40 The progress of the values of the objective functions used for trajectory tracking and heading control of particular robots in the experiment presented in Subsection 7.1.4 - variable segmented trajectory.

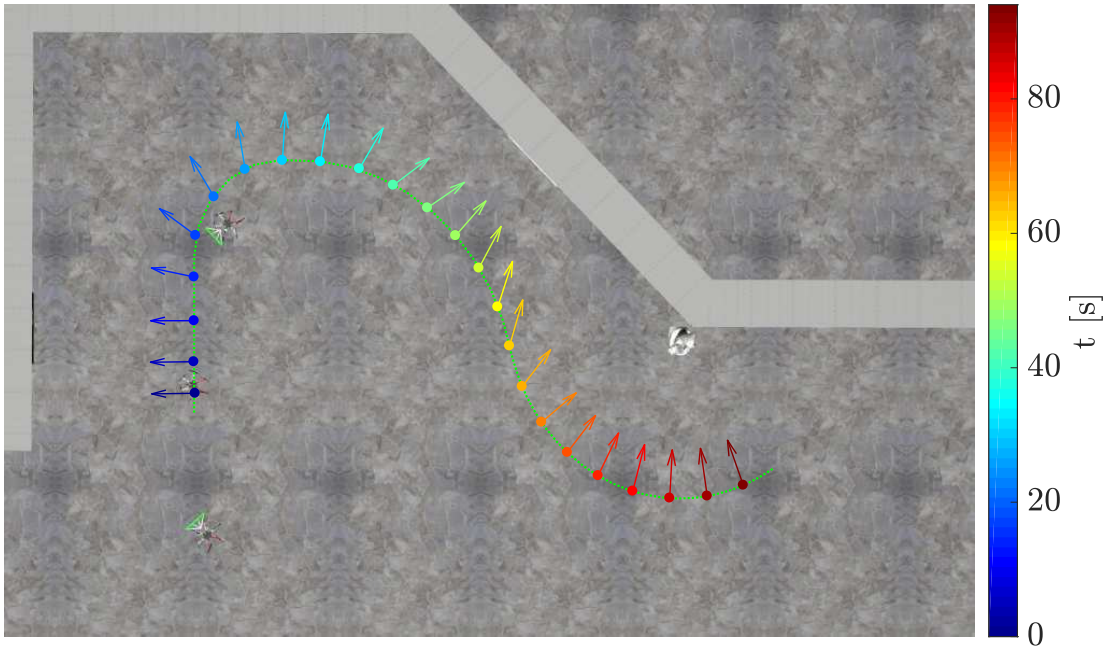

Fig. 41 The trajectory of the leader in the experiment in simple environment - trajectory with constant step presented in Subsection 7.1.4. The arrows denote the camera heading at particular times t, and the green dotted line shows the desired trajectory.

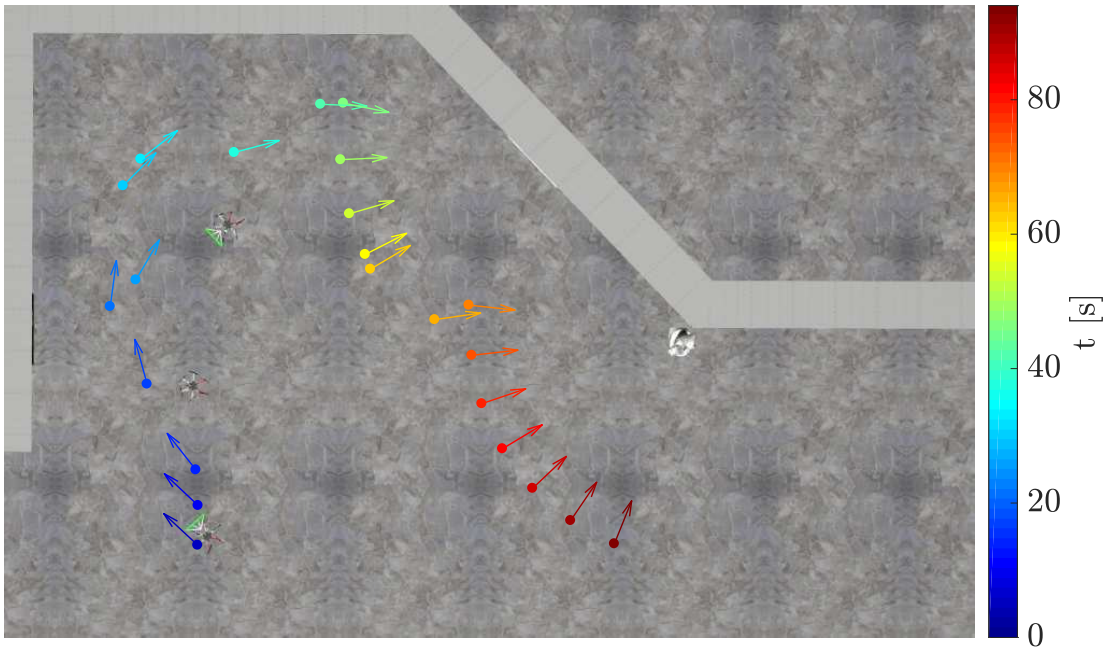

Fig. 42 The trajectory of the follower carrying the key light in the experiment in simple environment - trajectory with constant step presented in Subsection 7.1.4. The arrows denote the heading of light at particular times t, and the green dotted line shows the desired trajectory.

Fig. 43 The trajectory of the follower carrying the fill light in the experiment in simple environment - trajectory with constant step presented in Subsection 7.1.4. The arrows denote the heading of light at particular times t, and the green dotted line shows the desired trajectory.

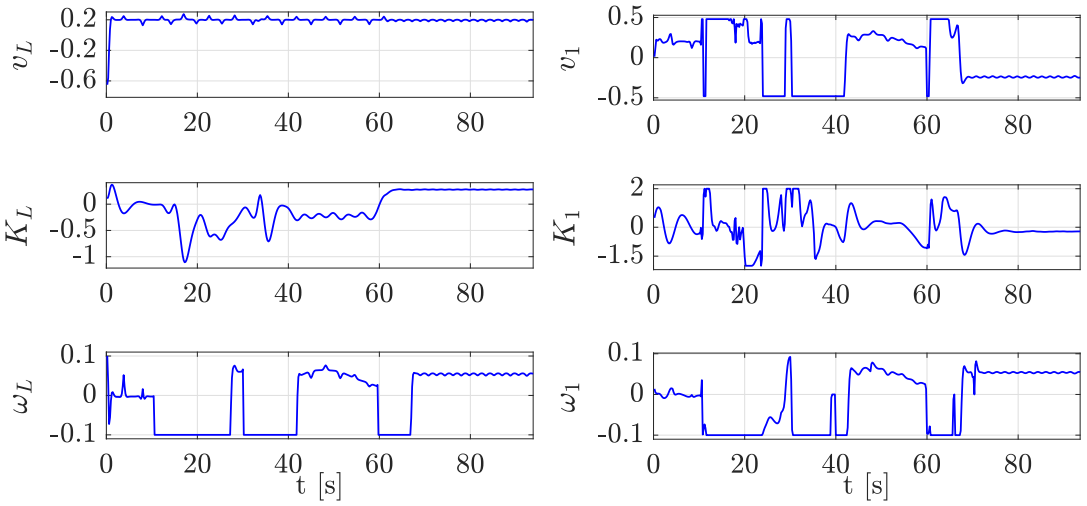

a) leader with camera **b)** follower with key light

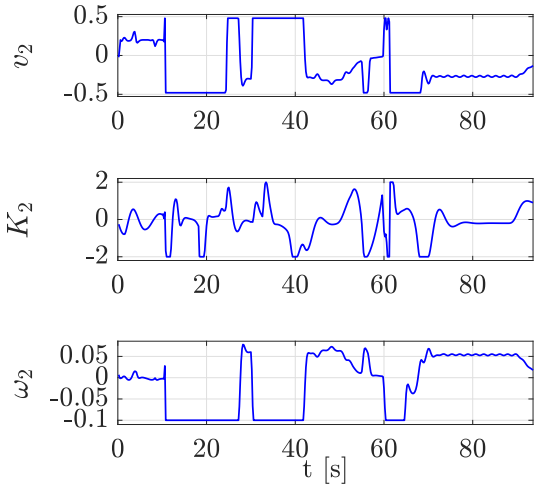

c) follower with fill light

Fig. 44 Control inputs used for controlling of the robots in the experiment presented in Subsection 7.1.4 - trajectory with constant step.

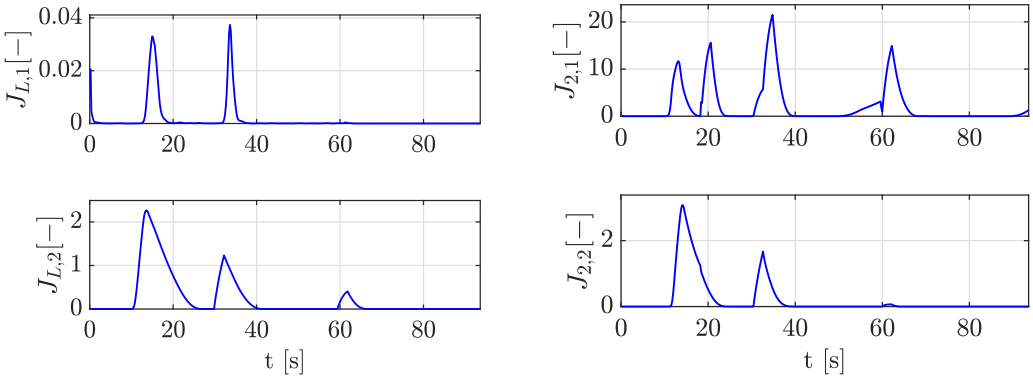

a) leader carrying the camera

b) follower carrying the key light

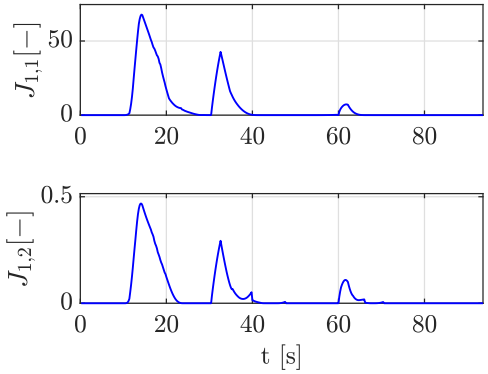

c) follower carrying the fill light

Fig. 45 The progress of the values of the objective functions used for trajectory tracking and heading control of particular robots in the experiment presented in Subsection 7.1.4 - trajectory with constant step.

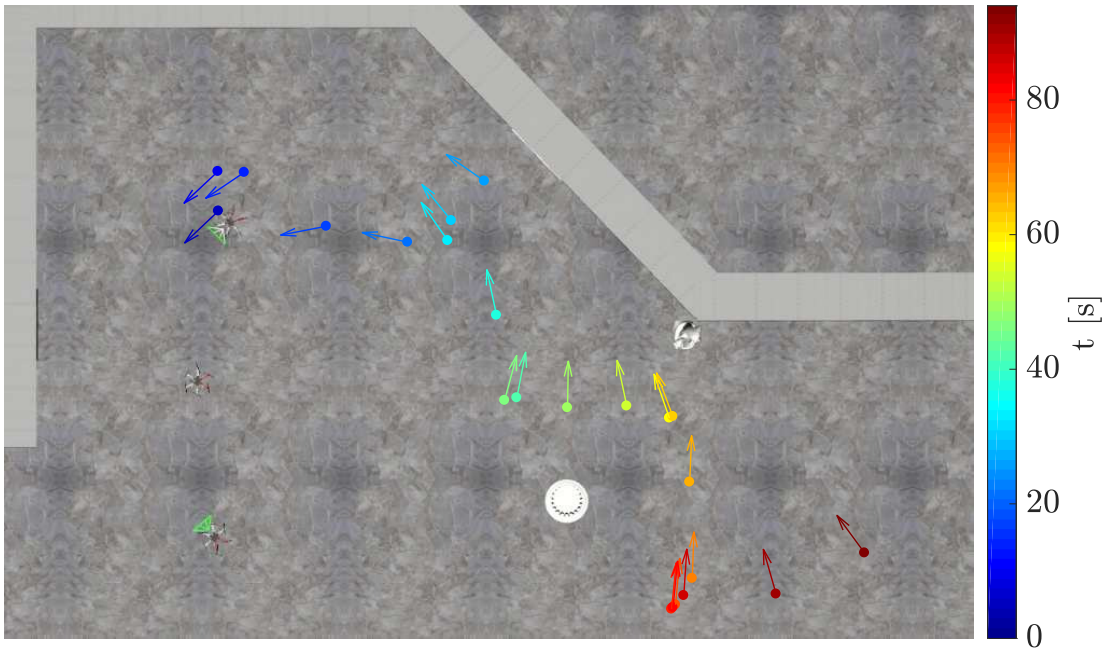

Fig. 46 The trajectory of the follower carrying the fill light in the experiment in simple environment with the obstacle. The arrows denote the heading of light at particular times t.

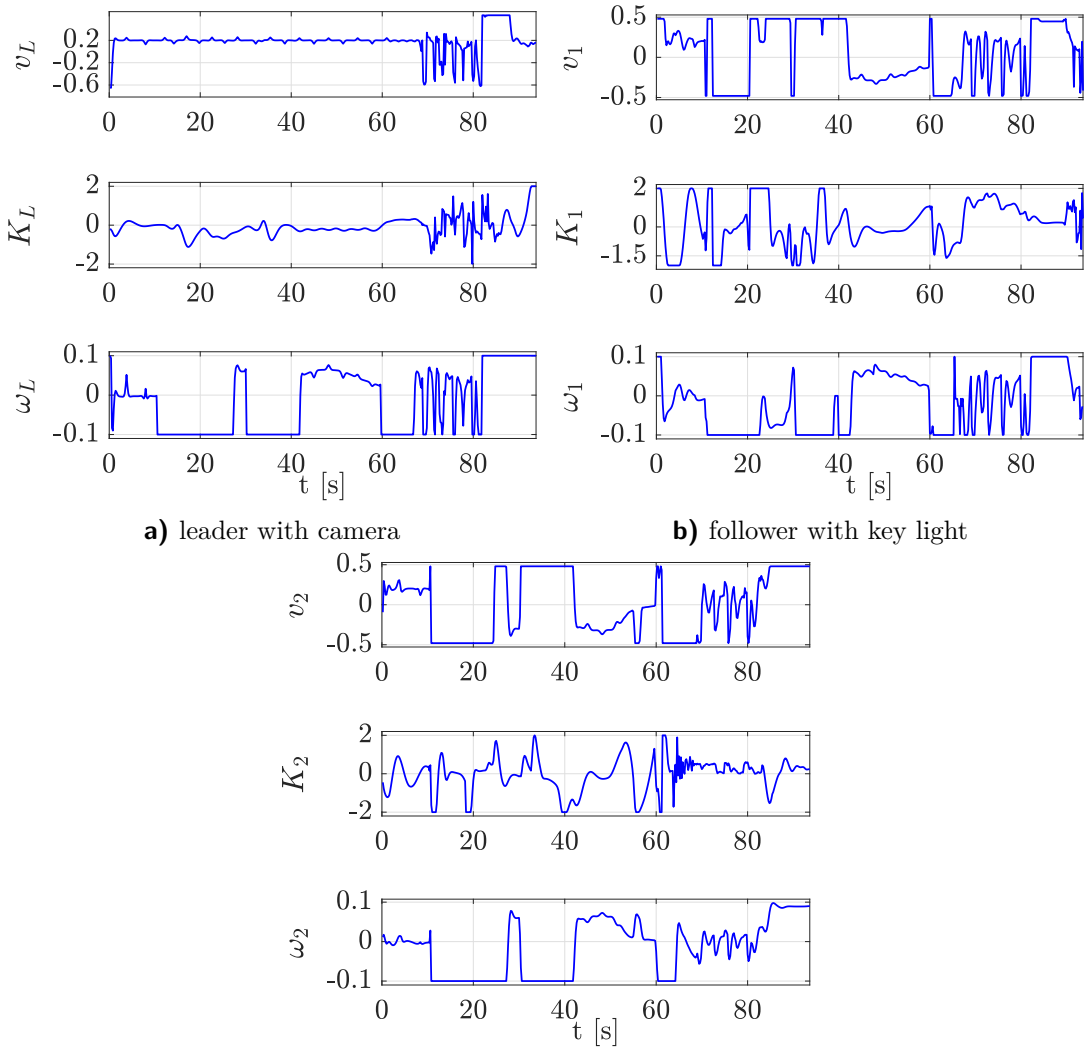

a) leader with camera **b)** follower with key light

c) follower with fill light

Fig. 47 Control inputs used for controlling of the robots in the experiment with the obstacle presented in Subsection 7.1.4.

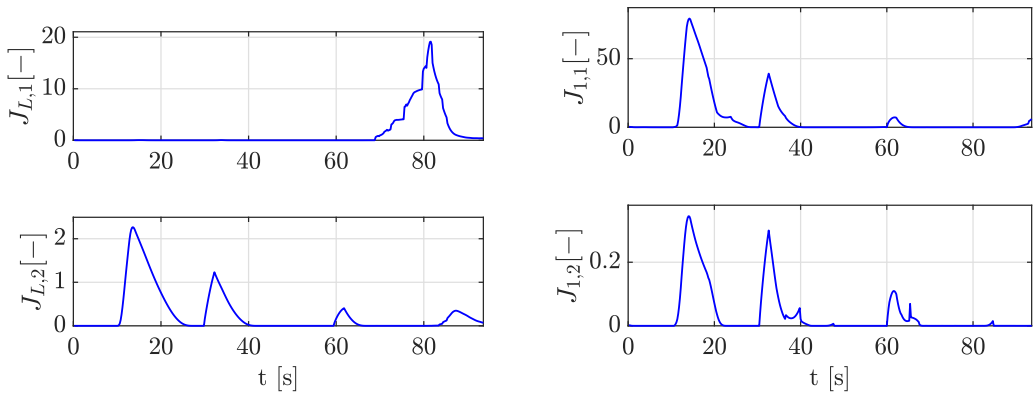

a) leader carrying the camera **b)** follower carrying the key light

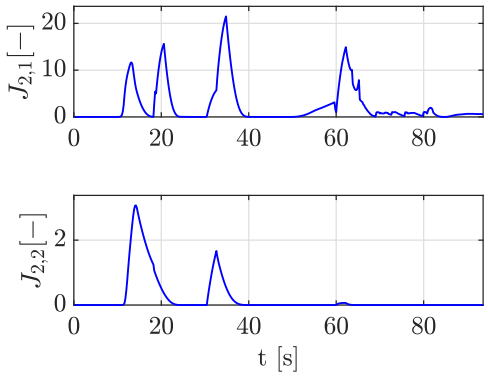

c) follower carrying the fill light

Fig. 48 The progress of the values of the objective functions used for trajectory tracking and heading control of particular robots in the experiment with the obstacle presented in Subsection 7.1.4.